New Folder Name Binary Inspiral

Observing binary inspiral in gravitational radiation: One interferometer

Lee Samuel Finn
Department of Physics and Astronomy,
Northwestern University, Evanston, Illinois 60208

David F. Chernoff
Department of Astronomy, Cornell University,
Ithaca, New York 14853
(18 November 1992)

Abstract

Close binary systems of compact objects with less than ten minutes remaining before coalescence are readily identifiable sources of gravitational radiation for the United States Laser Interferometer Gravitational-wave Observatory (LIGO) and the French-Italian VIRGO gravitational-wave observatory. As a start toward assessing the full capabilities of the LIGO/VIRGO detector network, we investigate the sensitivity of individual LIGO/VIRGO-like interferometers and the precision with which they can determine the characteristics of an inspiralling binary system. Since the two interferometers of the LIGO detector share nearly the same orientation, their joint sensitivity is similar to that of a single, more sensitive interferometer. We express our results for a single interferometer of both initial and advanced LIGO design, and also for the LIGO *detector* in the limit that its two interferometers share exactly the same orientation.

We approximate the secular evolution of a binary system as driven exclusively by its leading order quadrupole gravitational radiation. Observations of a binary in a single interferometer are described by four characteristic quantities: an amplitude $\mathcal{A}$, a chirp mass $\mathcal{M}$, a time T, and a phase ψ. We find the amplitude signal-to-noise ratio (SNR) ρ of an observed binary system as a function of $\mathcal{A}$ and $\mathcal{M}$ for a particular orientation of the binary with respect to the interferometer, and also the distribution of SNRs for randomly oriented binaries at a constant distance To assess the interferometer sensitivity, we calculate the rate at which sources are expected to be observed and the range to which they are observable. Assuming a conservative rate density for coalescing neutron star binary systems of $8 \times 10^{-8}\,\mathrm{yr}^{-1}\,\mathrm{Mpc}^{-3}$, we find that the advanced LIGO detector will observe approximately 69 yr^{-1} with an amplitude SNR greater than 8. Of these, approximately 7 yr^{-1} will be from binaries at distances greater than 950 Mpc.

We give analytic and numerical results for the precision with which each of the characteristic quantities can be determined by interferometer observations. For neutron star binaries, the fractional one-sigma statistical error in the determination of $\mathcal{A}$ is equal to $1/\rho$. For $\rho > 8$, the fractional one-sigma error in the measurement of $\mathcal{M}$ in the advanced LIGO detectors is less than 2×10^{-5}, a phenomenal precision. The characteristic time is related to the moment when coalescence occurs, and can be measured in the advanced detectors with a one-sigma uncertainty of less than 3×10^{-4} s (assuming $\rho > 8$).

We also explore the sensitivity of these results to a tunable parameter in the interferometer design (the recycling frequency). The optimum choice of the parameter is dependent on the goal of the observations, *e.g.*, maximizing the rate of detections or maximizing the precision of measurement. We determine the optimum parameter values for these two cases.

The calculations leading to the SNR and the precision of measurement assume that the interferometer observations extend over only the last several minutes of binary inspiral, during which time the orbital frequency increases from approximately 5 Hz to 500 Hz. We examine the sensitivity of our results to the elapsed time of the observation and show that observations of longer duration lead to very little improvement in the SNR or the precision of measurement.

PACS numbers: 04.80.+z,04.30+x,97.60.Jd,06.20.Dk

I. INTRODUCTION AND MOTIVATION

Both the United States Laser Interferometer Gravitational-wave Observatory (*LIGO* [1,2]) and the French/Italian VIRGO gravitational-wave observatory [3] are expected to begin operation in the late 1990s. Inspiralling binary systems of compact objects — either neutron stars or stellar mass black holes with orbital frequencies ranging from 5 s^{-1} to 500 s^{-1} — are currently regarded as the most certain observable source for these detectors: the density of sources [4,5] suggest event rates of several per year and the radiation they emit can be calculated unambiguously [6–12]. In support of the LIGO/VIRGO observational effort, theoreticians must combine refined calculations of the radiation from binary inspiral with the anticipated detector properties to deduce the instrument sensitivity. These calculations will, in turn, play an important role in the final design and ultimate use of the instruments. In this paper, we begin a detailed analysis of binary inspiral as a source of gravitational radiation for a LIGO/VIRGO-like interferometric detector.

Our goal in this work is to estimate the sensitivity of LIGO/VIRGO-like interferometers and the LIGO detector by determining the rate at which inspiralling binary systems can be detected, the range to which they can be observed, and the precision with which they can by characterized in a single interferometer. We also explore the compromises that must be made as different questions are asked of the observations. The optimal design and operation of these interferometers depends on a detailed understanding of the nature of the detector response to the radiation, the detector noise power spectral density (PSD), *and the questions the observation is meant to resolve.* For example, we show in §V that the goal of observing as many sources as possible (without necessarily being able to characterize them precisely) leads to a different optimal interferometer configuration than the goal of characterizing observed sources as precisely as possible (while allowing that weak sources may be missed entirely).

The ultimate goal of our assessment of binary inspiral is to determine the ability of a single interferometer (or a network of such interferometers) to

1. *Detect* the gravitational radiation from the last few minutes of inspiral of a binary neutron star or black hole system, and

2. *Measure* the parameters describing the detected binary system from the observed gravitational radiation.

By *detection* we mean the determination of the presence or absence of a signal characteristic of an inspiralling binary system in the output of a detector, *irrespective* of the particular parameters that might characterize the observed binary system. By *measurement* we mean the determination of the parameters that characterize the signal *presumed to be present* in the detector output. In a real detector noise can mask or distort a signal present in the detector output; alternatively, it can conspire to appear as a signal characteristic of a binary system. Consequently, any conclusion we draw from observations (*e.g.*, that we have detected an inspiralling binary system) is associated with a probability that characterizes our certainty in its validity.

As a practical matter, reliable detection of gravitational radiation will initially require coincident observation between two or more interferometers so that non-Gaussian noise events can be differentiated from gravitational radiation signals. When completed, the

LIGO *detector* will consist of two *interferometers:* one in Hanford, Washington and one in Livingston, Louisiana [2]. The relative orientation of the two interferometers has been chosen to maximize their sensitivity to a single polarization state of the gravitational radiation impinging on the Earth[1] [13]; consequently, the two interferometers act together like a single interferometer whose sensitivity will be greater than that of either of its components. This analogy is not exact: combining the interferometers in this way ignores the different arrival times of the signal at the two distinct interferometers. Nevertheless, our single-detector analysis is directly relevant to the actual LIGO configuration, and we discuss our results in the context of *(i)* single LIGO/VIRGO-like *interferometers* of the proposed initial and advanced designs, and *(ii)* the LIGO *detector* in the limit that its two independent interferometers share exactly the same orientation and ignoring the difference in the signal arrival times.

In principle, simultaneous observation of an inspiralling binary system in *three* interferometers of different orientations is sufficient to measure (among other characteristics) the binary's luminosity distance d_L, its position in the sky, and a function $\mathcal{M}$ that depends only on the masses of its components and its cosmological redshift [14,15]. If the position is known through other observations, then $\mathcal{M}$ and d_L can be measured from observations with only two interferometers of different orientations. Observation of an inspiralling binary in a single interferometer can measure $\mathcal{M}$ and a waveform "amplitude" $\mathcal{A}$, which depends on the luminosity distance and orientation of the binary with respect to the detector. Even this limited information is of astrophysical significance, however: from observations of the distribution of $\mathcal{A}$ and $\mathcal{M}$ among the observed binaries one can determine the distribution of the component masses of inspiralling binary systems, find the Hubble constant and deceleration parameter, and test cosmological models [16].

The study of binary systems as sources of gravitational radiation began in 1963 when Peters and Mathews [6] made the first detailed calculation of the gravitational radiation luminosity from inspiralling binary systems, focusing on the leading order quadrupole radiation from two point particles in circular and elliptical orbits. Clark and Eardley [17] explored how gravitational radiation (among other effects) drives the orbital evolution of binary systems. Clark [18] suggested inspiralling binary systems as an important source of gravitational radiation for modern interferometric detectors; however, he considered only the burst of radiation from the coalescence event itself. Thorne recognized the importance of the gravitational radiation from the final few minutes of *inspiral.* Since 1987 a number of investigators have worked with increasing sophistication on problems related to the observation of inspiralling binaries in interferometric detectors. Some have focused on understanding and refining interferometer detector technology [19–24], others have focused on the data analysis problems of detecting or determining the characteristics of a binary system from the radiation [25–30], and still others have focused on refining our understanding of the gravitational radiation waveform from these systems [7–12,31–33] or their rate of occurrence

---

[1]While primarily sensitive to a single polarization state of the radiation field, LIGO will, with more limited sensitivity, be capable of observing both polarizations simultaneously. In a subsequent paper we will take the exact detector orientations into account in our analysis.

in the Universe [4,5].

The remainder of this paper is organized as follows. In §II we review how the precision with which the parameterization of a signal, observed in a noisy detector, is determined. In §III, we apply these techniques to the particular problem of finding the precision with which the parameters of an inspiralling binary system can be measured. These results depend only on the detector noise power spectral density (PSD) and not on the type of detector (*e.g.*, interferometer or bar). In §IV we apply the results of §III to both the initial and advanced proposed LIGO/VIRGO-like interferometers. We discuss the astrophysical implications of these results in §V and present our conclusions in §VI.

II. MEASUREMENT AND UNCERTAINTY

In this section we review the techniques we use to determine the statistical uncertainties in observations of binary inspiral. A complete discussion is found in Finn [34]. The techniques developed there are closely related to those associated with signal analysis by optimal filtering. For more information on optimal filtering and signal analysis we direct the reader to Oppenheim, Willsky, and Young [35], the review by Davis [36] and references therein, Wainstein and Zubakov [37], and Hancock and Wintz [38].

A. Introduction

Consider a deterministic (*i.e*, not stochastic) source of gravitational radiation (*e.g.*, an inspiralling binary system) and a detector (*e.g.*, a laser interferometer). We write the response of the detector to the radiation as a superposition of noise $n(t)$ and signal $m(t;\boldsymbol{\mu})$, where $\boldsymbol{\mu}$ is a minimal set of parameters that uniquely characterizes the detector response (absent the noise) to the radiation for the entire duration of the observation (in §III we show that for an inspiralling binary system observed by a single interferometric detector $\boldsymbol{\mu}$ is a four dimensional vector). Let the source of radiation be characterized by $\tilde{\boldsymbol{\mu}}$. In analyzing the output of the detector, we have two goals:

1. To determine whether a signal is present in the detector output, and

2. To find the precision with which we can determine $\tilde{\boldsymbol{\mu}}$ (assuming a signal is present).

Owing to the detector noise, we cannot determine with certainty either the presence of a signal or (assuming it present) $\tilde{\boldsymbol{\mu}}$. Instead, we find the probability that the detector output is consistent with the presence of a signal, and represent our uncertainty in $\tilde{\boldsymbol{\mu}}$ by a set of volumes $V(P)$ in parameter space, such that $\tilde{\boldsymbol{\mu}}$ is in $V(P)$ with probability P. The volumes $V(P)$ are a measure of the sensitivity of the detector. Throughout this section, we will assume that we have determined that a signal is present so that the probability P associated with $V(P)$ is a conditional probability. In a later paper, we will discuss the determination of the probability that a signal of the form $m(t;\boldsymbol{\mu})$ is present in the detector output.

Each observed signal is immersed in its own realization of the detector noise; consequently we cannot know in advance of an observation what the volumes $V(P)$ will look like. We can.

however, determine what the most likely volumes are for a given observation, and that is what we do here. In this section we review briefly the procedures used to find the most likely volumes $V(P)$. These procedures are developed in Finn [34], and we refer the interested reader there for more information.

B. The probability volumes $V(P)$

We characterize the observed output of our detector as a time series $g(t)$, which is a superposition of noise $n(t)$ and (perhaps) a signal $m(t;\tilde{\boldsymbol{\mu}})$:

$$g(t) \equiv \begin{cases} n(t) + m(t;\tilde{\boldsymbol{\mu}}) & \text{signal present} \\ n(t) & \text{signal absent.} \end{cases} \tag{2.1}$$

The parameter $\tilde{\boldsymbol{\mu}}$ is fixed but unknown, and we assume the noise is drawn from a stationary process. The probability density that a signal with parameterization $\boldsymbol{\mu}$ is present in the detector output $g(t)$ is

$$\begin{aligned} P(\boldsymbol{\mu}|g) &\equiv \begin{pmatrix} \text{The conditional probability that a} \\ \text{signal characterized by } \boldsymbol{\mu} \text{ is present} \\ \text{given the detector output } g(t). \end{pmatrix} \\ &= \frac{\Lambda(\boldsymbol{\mu})}{\Lambda + P(0)/P(m)} \end{aligned} \tag{2.2}$$

where

$$P(0) \equiv \begin{pmatrix} \text{The } \textit{a priori} \text{ probability} \\ \text{that the signal is absent} \end{pmatrix}, \tag{2.3a}$$

$$P(m) \equiv \begin{bmatrix} \text{The } \textit{a priori} \text{ probability} \\ \text{that the signal } m(\boldsymbol{\mu}) \\ \text{(for undetermined } \boldsymbol{\mu}) \\ \text{is present} \end{bmatrix}, \tag{2.3b}$$

$$\Lambda \equiv \int d^N\mu\, \Lambda(\boldsymbol{\mu}), \tag{2.3c}$$

$$\Lambda(\boldsymbol{\mu}) \equiv p(\boldsymbol{\mu}) \exp\left[2\left\langle g, m(\boldsymbol{\mu})\right\rangle - \left\langle m(\boldsymbol{\mu}), m(\boldsymbol{\mu})\right\rangle\right], \tag{2.3d}$$

$$p(\boldsymbol{\mu}) \equiv \begin{pmatrix} \text{The } \textit{a priori} \text{ probability} \\ \text{density that the signal} \\ \text{parameterization is } \boldsymbol{\mu}. \end{pmatrix}, \tag{2.3e}$$

$$\langle r, s\rangle \equiv \int_{-\infty}^{\infty} df\, \frac{\tilde{r}(f)\tilde{s}^*(f)}{S_h(|f|)}, \tag{2.3f}$$

$$\tilde{r}(f) \equiv \int_{-\infty}^{\infty} dt\, e^{2\pi i f t} r(t), \tag{2.3g}$$

$$S_h(f) \equiv \begin{bmatrix} \text{One-sided detector noise} \\ \text{power spectral density (PSD)} \end{bmatrix}. \tag{2.3h}$$

The *likelihood ratio* Λ (eqn. 2.3c) is proportional to the *a posteriori* probability that a signal is present in the observed $g(t)$. When that probability exceeds a given threshold we assume a signal is present and try to determine $\tilde{\boldsymbol{\mu}}$. We characterize an observation of $g(t)$ in terms of the mode (*i.e.*, the maximum) of the distribution $P(\boldsymbol{\mu}|g)$, denoted $\hat{\boldsymbol{\mu}}$. The mode of $P(\boldsymbol{\mu}|g)$ is also the mode of the *odds ratio* $\Lambda(\boldsymbol{\mu})$. In terms of $\hat{\boldsymbol{\mu}}$ the observation's signal-to-noise ratio (SNR) ρ^2 is[2]

$$\rho^2 = 2\left\langle m(\hat{\boldsymbol{\mu}}), m(\hat{\boldsymbol{\mu}})\right\rangle . \tag{2.4}$$

Assuming that $\Lambda(\boldsymbol{\mu})$ is smooth and that its global maximum is a local extremum, $\hat{\boldsymbol{\mu}}$ satisfies

$$2\left\langle m(\tilde{\boldsymbol{\mu}}) - m(\hat{\boldsymbol{\mu}}), \frac{\partial m}{\partial \mu_j}(\hat{\boldsymbol{\mu}})\right\rangle + \frac{\partial \ln p}{\partial \mu_j}(\hat{\boldsymbol{\mu}}) = -2\left\langle n, \frac{\partial m}{\partial \mu_j}(\hat{\boldsymbol{\mu}})\right\rangle . \tag{2.5}$$

We assume that the noise $n(t)$ is a normal random variable with zero mean; consequently, so are each of the $\langle n, \partial m/\partial \mu_j\rangle$ on the righthand side of equation 2.5. Denote these random variables ν_i:

$$\nu_i \equiv 2\left\langle n, \frac{\partial m}{\partial \mu_i}(\hat{\boldsymbol{\mu}})\right\rangle . \tag{2.6}$$

Since the ν_i are normal, their joint distribution is a multivariate Gaussian, characterized by the means $\overline{\nu_i}$, which vanish, and the quadratic moments

$$\overline{\nu_i \nu_j} = 4\overline{\left\langle n, \frac{\partial m}{\partial \mu_i}(\hat{\boldsymbol{\mu}})\right\rangle \left\langle n, \frac{\partial m}{\partial \mu_j}(\hat{\boldsymbol{\mu}})\right\rangle}$$

$$= 2\left\langle \frac{\partial m}{\partial \mu_i}(\hat{\boldsymbol{\mu}}), \frac{\partial m}{\partial \mu_j}(\hat{\boldsymbol{\mu}})\right\rangle \tag{2.7a}$$

$$\equiv \mathcal{C}_{ij}^{-1}. \tag{2.7b}$$

Here we have used an overbar to indicate an average over all instances of the noise $n(t)$. Since we have assumed that the noise is normal these averages can be evaluated using the ergodic theorem (*cf.* Finn [34] for more details). In terms of $\mathcal{C}_{ij}$ (*i.e.*, the inverse of $\mathcal{C}_{ij}^{-1}$), the joint distribution of the ν_i is given by the probability density

$$p(\boldsymbol{\nu}) = \frac{\exp\left[-\frac{1}{2}\sum_{i,j}\mathcal{C}_{ij}\nu_i\nu_j\right]}{\left[(2\pi)^N \det||\mathcal{C}_{ij}^{-1}||\right]^{1/2}} \tag{2.8}$$

---

[2]Note that ρ^2 is quadratic in the signal strength. In the literature SNR is often used to refer to both ρ and ρ^2. We avoid this ambiguity by using either ρ or ρ^2 as appropriate.

This is also the joint distribution of the quantities that appear on the lefthand side of equation 2.5. In Finn [34] it was stated that for an observation characterized by $\hat{\boldsymbol{\mu}}$, the probability volumes $V(P)$ are given implicitly by

$$K^2 \geq \sum_{i,j} \mathcal{C}_{ij} \left[2 \left\langle m(\boldsymbol{\mu}) - m(\hat{\boldsymbol{\mu}}), \frac{\partial m}{\partial \mu_i}(\hat{\boldsymbol{\mu}}) \right\rangle + \frac{\partial \ln p}{\partial \mu_i}(\hat{\boldsymbol{\mu}}) \right] \times \left[2 \left\langle m(\boldsymbol{\mu}) - m(\hat{\boldsymbol{\mu}}), \frac{\partial m}{\partial \mu_j}(\hat{\boldsymbol{\mu}}) \right\rangle + \frac{\partial \ln p}{\partial \mu_j}(\hat{\boldsymbol{\mu}}) \right], \tag{2.9}$$

where

$$P = \int_{\sum_{i,j} \mathcal{C}_{ij} \nu_i \nu_j \leq K^2} d^N \nu \frac{\exp\left[-\frac{1}{2} \sum_{i,j} \mathcal{C}_{ij} \nu_i \nu_j \right]}{\left[(2\pi)^N \det ||\mathcal{C}_{ij}^{-1}|| \right]^{1/2}} \tag{2.10}$$

and $\tilde{\boldsymbol{\mu}} \in V(P)$ with probability P (recall that P is conditional on the assumption that a signal is in fact present in the detector output). *This is correct only when $\Lambda(\boldsymbol{\mu})$ has a single extremum, or near $\hat{\boldsymbol{\mu}}$.* In the most general case only a Monte Carlo analysis can determine the probability volumes $V(P)$. No other results of Finn [34] are affected by this correction.

C. The strong signal approximation

The volumes $V(P)$ are representations of a cumulative probability distribution function. Denote the corresponding probability density by $P(\delta\boldsymbol{\mu}|\hat{\boldsymbol{\mu}})$:

$$P(\delta\boldsymbol{\mu}|\hat{\boldsymbol{\mu}}) \equiv \begin{pmatrix} \text{The conditional probability} \\ \text{density that } m \text{ is characterized} \\ \text{by } \hat{\boldsymbol{\mu}} + \delta\boldsymbol{\mu}, \text{ given that } \Lambda(\boldsymbol{\mu}) \\ \text{has mode } \hat{\boldsymbol{\mu}} \end{pmatrix} \tag{2.11}$$

In the limit of large ρ^2, $P(\delta\boldsymbol{\mu}|\hat{\boldsymbol{\mu}})$ becomes sharply peaked about $\hat{\boldsymbol{\mu}}$ and the determination of $V(P)$ is greatly simplified. Suppose that ρ^2 is so large that for $\tilde{\boldsymbol{\mu}} \in V(P)$ for all P of interest the difference $m(\tilde{\boldsymbol{\mu}}) - m(\hat{\boldsymbol{\mu}})$ can be linearized in $\delta\boldsymbol{\mu}$, where

$$\delta\boldsymbol{\mu} \equiv \tilde{\boldsymbol{\mu}} - \hat{\boldsymbol{\mu}}. \tag{2.12}$$

We then obtain in place of equation 2.5

$$\sum_{i,j} \delta\mu_i \mathcal{C}_{ij}^{-1} = -2 \left\langle n, \frac{\partial m}{\partial \mu_j}(\hat{\boldsymbol{\mu}}) \right\rangle - \frac{\partial \ln p}{\partial \mu_j}(\hat{\boldsymbol{\mu}}) \tag{2.13}$$

The random variables $\delta\boldsymbol{\mu}$ are related to the $\boldsymbol{\nu}$ by a linear transformation,

$$\delta\mu_i = -\sum_{i,j} \mathcal{C}_{ij} \left[\nu_j + \frac{\partial \ln p}{\partial \mu_j}(\hat{\boldsymbol{\mu}}) \right]; \tag{2.14}$$

consequently, the $\delta\boldsymbol{\mu}$ are normal with means

$$\overline{\delta\mu_i} = -\sum_{i,j} \mathcal{C}_{ij} \frac{\partial \ln p}{\partial \mu_j}(\hat{\boldsymbol{\mu}}), \tag{2.15}$$

and quadratic moments

$$\overline{\left(\delta\mu_i - \overline{\delta\mu_i}\right)\left(\delta\mu_j - \overline{\delta\mu_j}\right)} = \mathcal{C}_{ij}. \tag{2.16}$$

The probability distribution $P(\delta\boldsymbol{\mu}|\hat{\boldsymbol{\mu}})$ is thus a multivariate Gaussian (*cf.* eqn. 2.8):

$$P(\delta\boldsymbol{\mu}|\hat{\boldsymbol{\mu}}) = \frac{\exp\left[-\frac{1}{2}\sum_{i,j}\mathcal{C}_{ij}^{-1}\left(\delta\mu_i - \overline{\delta\mu_i}\right)\left(\delta\mu_j - \overline{\delta\mu_j}\right)\right]}{\left[(2\pi)^N \det||\mathcal{C}_{ij}||\right]^{1/2}}. \tag{2.17}$$

Note that the matrix $\mathcal{C}_{ij}$ has now acquired a physical meaning: in particular, we see that the variances σ_i^2 of the $\delta\mu_i$ are

$$\begin{aligned}\sigma_i^2 &\equiv \overline{\left(\delta\mu_i - \overline{\delta\mu_i}\right)^2} \\ &= \mathcal{C}_{ii}\end{aligned} \tag{2.18}$$

and the correlation coefficients r_{ij} are given by

$$\begin{aligned}r_{ij} &\equiv \sigma_i^{-1}\sigma_j^{-1}\overline{\left(\delta\mu_i - \overline{\delta\mu_i}\right)\left(\delta\mu_j - \overline{\delta\mu_j}\right)} \\ &= \frac{\mathcal{C}_{ij}}{\sigma_i\sigma_j}\end{aligned} \tag{2.19}$$

In this sense we say that $\mathcal{C}_{ij}$ is the covariance matrix of the random variables $\delta\boldsymbol{\mu}$.

In the strong signal approximation, the surfaces bounding the volume $V(P)$ are ellipsoids defined by the equation

$$\sum_{i,j}\left(\delta\mu_i - \overline{\delta\mu_i}\right)\left(\delta\mu_j - \overline{\delta\mu_j}\right)\mathcal{C}_{ij}^{-1} = K^2, \tag{2.20}$$

where the constant K^2 is related to P by

$$P = \int_{\sum_{i,j}\mathcal{C}_{ij}^{-1}x^i x^j \le K^2} d^N x \, \frac{\exp\left[-\frac{1}{2}\sum_{i,j}\mathcal{C}_{ij}^{-1}x^i x^j\right]}{\left[(2\pi)^N \det||\mathcal{C}_{ij}||\right]^{1/2}} \tag{2.21}$$

Finally we come to the question of when the linearization in equation 2.13 is a reasonable approximation. Three considerations enter here:

1. The probability contours of interest (*e.g.*, 90%) must not involve $\delta\boldsymbol{\mu}$ so large that the linearization of $m(\tilde{\boldsymbol{\mu}}) - m(\hat{\boldsymbol{\mu}})$ is a poor approximation;

2. The probability contours of interest must not involve $\delta\boldsymbol{\mu}$ so large that for $\delta\boldsymbol{\mu} \in V(P)$, $\Lambda(\delta\boldsymbol{\mu} + \hat{\boldsymbol{\mu}})$ has more than one extremum or inflection point; and

3. The condition number of the matrix $\mathcal{C}_{ij}^{-1}$ must be sufficiently small that the inverse $\mathcal{C}_{ij}$ is insensitive to the linearization approximation in the neighborhood of $\hat{\boldsymbol{\mu}}$.[3]

If the validity of the linearization procedure for a particular problem is doubtful owing to the violation of any of these conditions, then we must fall-back on either equations 2.5, 2.9 and 2.10 (if $\Lambda(\boldsymbol{\mu})$ has a single extremum), or a Monte Carlo analysis.

III. PRECISION OF MEASUREMENT: BINARY INSPIRAL

In this section we apply the techniques described in §II to the problem of measuring the characteristics of an inspiralling binary system in an interferometric gravitational radiation detector. We determine the gravitational radiation from an evolving binary system in the quadrupole approximation and evaluate the corresponding detector response. The amplitude of the response is a function of the (unknown and unknowable) relative orientation of the source and the detector, and we evaluate its mean square amplitude and *a priori* cumulative probability distribution. We also discuss the validity of describing binary evolution using the quadrupole approximation, arguing that while the result is certainly not good enough for use in actual data analysis, it is sufficient for the purpose of exploring the precision with which we will ultimately be able to characterize a binary system through gravitational radiation observations in LIGO/VIRGO-like interferometers.

The general interferometer response to the gravitational radiation from an inspiralling binary system is a sinusoid with slowly varying amplitude and frequency. Using the stationary phase approximation, we obtain an analytic expression for the Fourier transform of the response. We find that the SNR ρ^2 and the covariance matrix $\mathcal{C}_{ij}$ can be expressed simply in terms of several moments of $S_h^{-1}(f)$, the inverse of the interferometer noise PSD.

A. Parameterization of the radiation waveform

In order to express the response of a single interferometer to the gravitational radiation from a binary system (or any source), we define two coordinate systems: the *source* coordinate system and the *radiation* coordinate system. The binary system is most simply described in the source coordinate system. The $\mathbf{e}_z^S$-axis of this coordinate system is along the binary system's angular momentum. We choose the axes $\mathbf{e}_x^S$ and $\mathbf{e}_y^S$ of the source coordinate system to make the expression of the radiation directed toward the interferometer simple: the $\mathbf{e}_x^S$ axis is chosen so that the unit vector $\mathbf{n}_I$ in the direction of the interferometer is in the $\mathbf{e}_x^S \wedge \mathbf{e}_z^S$ plane and in the positive $\mathbf{e}_x^S$ direction (if the interferometer is along the polar axis, then there is no preferred direction for the $\mathbf{e}_x^S$ axis).

---

[3]Recall that the relative error in $\delta\boldsymbol{\mu}$ is the condition number times the relative error in $\mathcal{C}_{ij}^{-1}$: for a large condition number, small errors in $\mathcal{C}_{ij}^{-1}$ introduced by the linearization approximation can result in large errors in $\delta\boldsymbol{\mu}$ (*cf.* Golub & Van Loan [39]).

The radiation coordinate system has its $\mathbf{e}_z^R$ axis in the direction $\mathbf{n}_I$, and its $\mathbf{e}_x^R$ and $\mathbf{e}_y^R$ axes are projections of the $\mathbf{e}_x^S$ and $\mathbf{e}_y^S$ coordinate axes normal to $\mathbf{n}_I$:

$$\mathbf{e}_y^R = \mathbf{e}_y^S, \tag{3.1a}$$

$$\mathbf{e}_x^R = \mathbf{e}_y^S \times \mathbf{n}_I. \tag{3.1b}$$

In the radiation coordinate system, the radiation propagating toward the interferometer is described by

$$\mathbf{h} = h_+ \mathbf{e}_+ + h_\times \mathbf{e}_\times \tag{3.2}$$

where

$$\mathbf{e}_+ = \mathbf{e}_x^R \otimes \mathbf{e}_x^R - \mathbf{e}_y^R \otimes \mathbf{e}_y^R \tag{3.3a}$$

$$\mathbf{e}_\times = \mathbf{e}_x^R \otimes \mathbf{e}_y^R + \mathbf{e}_y^R \otimes \mathbf{e}_x^R. \tag{3.3b}$$

1. The quadrupole waveform

In the quadrupole approximation[4],

$$h_+ \equiv 2\frac{\mathcal{M}}{d_L}\left(1+\cos^2 i\right)(\pi \mathcal{M} f)^{2/3}\cos\left(\Phi + \Psi\right) \tag{3.4a}$$

$$h_\times \equiv 4\frac{\mathcal{M}}{d_L}\cos i\,(\pi \mathcal{M} f)^{2/3}\sin\left(\Phi + \Psi\right) \tag{3.4b}$$

where

$$d_L \equiv \left(\text{Luminosity distance to binary}\right), \tag{3.5a}$$

$$\cos i \equiv \mathbf{n}_I \cdot \mathbf{e}_x^S, \tag{3.5b}$$

$$i \equiv \left(\begin{array}{l}\text{Inclination angle of orbital}\\ \text{angular momentum to line of}\\ \text{sight toward the interferometer.}\end{array}\right), \tag{3.5c}$$

$$\begin{aligned}\mathcal{M} &\equiv (\text{Chirp mass}),\\ &= (1+z)\,\mu^{3/5} M^{2/5},\end{aligned} \tag{3.5d}$$

$$\Phi \equiv -2\left(\frac{T-t}{5\mathcal{M}}\right)^{5/8}, \tag{3.5e}$$

$$\begin{aligned}f &\equiv \frac{1}{2\pi}\frac{\partial \Phi}{\partial t},\\ &= \frac{1}{\pi \mathcal{M}}\left[\frac{5}{256}\frac{\mathcal{M}}{T-t}\right]^{3/8},\end{aligned} \tag{3.5f}$$

---

[4]Here and henceforth we adopt units where $G = c = 1$

Ψ is the phase of the binary system at $t = T$, T is the Newtonian "moment of coalescence," z is the cosmological redshift of the binary system, and M and μ are the binary system's total and reduced mass [6,40]. The gravitational radiation frequency f is twice the systems orbital frequency.

2. The interferometer response

The response of an interferometer to the gravitational radiation field is a linear combination of h_+ and $h_\times$:

$$m = F_+ h_+ + F_\times h_\times, \tag{3.6}$$

where the *antenna patterns* F_+ and $F_\times$ depend on the orientation of the interferometer with respect to the binary system [40]. We make no assumptions regarding the relative orientation of the interferometer and the binary; consequently, the general interferometer response is

$$m(t; \mathcal{A}, \mathcal{M}, \psi, T) \equiv \mathcal{A}\mathcal{M}\,(\pi f \mathcal{M})^{2/3} \cos\left(\Phi + \psi\right), \tag{3.7}$$

where ψ is a constant (distinct from Ψ in equations 3.4a and 3.4b), and Φ and f are given above in equations 3.5e and 3.5f. We will return in §III E to discuss how $\mathcal{A}$ depends on the orientation angles through F_+ and $F_\times$.

3. Radiation reaction and the quadrupole approximation

LIGO/VIRGO-like interferometers are most sensitive to gravitational radiation with frequencies in the range 30–1000 Hz. This corresponds to binary orbital frequencies of 15–500 Hz. In this regime gravitational radiation reaction is the most important factor in determining the evolution of a binary system's orbit [31,32]. In §III A 1, where we describe the evolution of the binary systems orbit, only backreaction owing to the leading-order quadrupole radiation is taken into account [6,40]. This approximation neglects higher order effects (in both v/c and M/r) that contribute to the gravitational radiation luminosity and, consequently, the evolution of f. This has serious ramifications for the construction of the model detector response [41].

The detector response to binary inspiral is a sinusoid of slowly varying amplitude and frequency. The determination of the characteristics of the binary system is equivalent to finding the "template" response that is most closely correlated to the detector response. If the phase of the template drifts from that of the signal by as little as π radians over the course of the observations, then the correlation will be insignificant. Neutron star binary inspiral observations in LIGO/VIRGO-like interferometers will last for on order $2\pi \times 10^4$ radians in phase; consequently, the phase advance can be determined to better than 1 part in 10^4. The errors we have made in our template $m(\boldsymbol{\mu})$ (eqn. 3.7) by neglecting the post-Newtonian contributions to the evolution of the binary system lead to phase differences significantly greater than 2π radians over 10^4 cycles observed. Consequently, the waveform model used in

actual data analysis must be more accurate than that given by the quadrupole approximation [42,41][5].

Nevertheless, for the particular purpose of exploring our ability to detect and characterize binary systems by their gravitational radiation signature, we believe the quadrupole approximation waveform is a useful substitute for a more accurate waveform. The determination of the *anticipated* sensitivity of a LIGO/VIRGO-like interferometer to binary inspiral depends on the ρ^2 and $\mathcal{C}_{ij}$, and we expect that the quadrupole approximation provides good lower bounds on these. The predominant observable effect of the inclusion of post-Newtonian corrections is to change the rate that the wave frequency f advances, thus changing the elapsed phase of the wave over the period of the observation. The SNR ρ^2 depends approximately on the elapsed phase and the corrections, while large compared to 2π, change this by only a small fraction of the total. Similarly, in the quadrupole approximation the rate at which f advances depends exclusively on $\mathcal{M}$ (*cf.* eqn. 3.5f); consequently, to the extent that the corrections to the quadrupole formula depend on characteristics of the binary other than $\mathcal{M}$ (*e.g.,* component masses and spins) these characteristics are observable and affect the precision with which $\mathcal{M}$ can be measured. In this way we expect that the use of a more accurate waveform in our analysis will increase the estimated $\sigma_{\mathcal{M}}$ but have little effect on our estimates of $\sigma_{\mathcal{A}}$, σ_{ψ}, and $\sigma_{\mathcal{T}}$ made using the quadrupole waveform and corresponding binary evolution.

B. The stationary phase approximation

In order to evaluate the SNR ρ^2 (eqn. 2.4) and the covariance matrix $\mathcal{C}_{ij}$ (eqn. 2.7b) we must find the Fourier transform $\widetilde{m}$ of m (eqn. 3.7). We approximate $\widetilde{m}$ using the method of stationary phase. Given a real function of the form

$$k(t) = A(t)\cos\hat{\Phi}(t), \tag{3.8}$$

where $\partial\hat{\Phi}/\partial t$ is a monotonically increasing function of t, the stationary phase approximation to the Fourier transform $\tilde{k}(f)$ is

$$\tilde{k}(f) = \int_{-\infty}^{\infty} dt\, k(t) e^{2\pi i f t} \tag{3.9a}$$

$$\simeq \begin{cases} \frac{1}{2}A\left[\mathcal{T}(f)\right]\left[2\pi/\frac{\partial^2\hat{\Phi}}{\partial t^2}[\mathcal{T}(f)]\right]^{1/2} & \\ \qquad \times \exp\left[i\left(2\pi f\mathcal{T}(f) - \hat{\Phi}(\mathcal{T}(f)) + \pi/4\right)\right] & \text{for } f > 0 \\ \tilde{k}^*(-f) & \text{for } f < 0, \end{cases} \tag{3.9b}$$

---

[5]Cutler, Finn, Poisson, and Sussman [42] have shown that successive post-Newtonian approximations to the evolution and waveform converge very slowly upon the fully relativistic solution. Consequently, it may require an impractically high order post-Newtonian expansion to predict correctly the advance of the phase over the course of the LIGO/VIRGO observations.

where

$$\mathcal{T}\left[\frac{1}{2\pi}\frac{\partial\hat{\Phi}}{\partial t}(t)\right] = t. \tag{3.10}$$

The validity of the approximation rests on the assumption that the amplitude A and the angular frequency $\partial\hat{\Phi}/\partial t$ change slowly over a period:

$$\frac{\partial \ln A/\partial t}{\partial\hat{\Phi}/\partial t} \ll 1 \qquad \text{and} \tag{3.11a}$$

$$\frac{\partial^2\hat{\Phi}/\partial t^2}{\left(\partial\hat{\Phi}/\partial t\right)^2} \ll 1. \tag{3.11b}$$

For the interferometer response m given in equation 3.7 these two relations are equivalent to the single condition

$$\frac{T-t}{\mathcal{M}} \gg \left(\frac{3\pi}{8}\right)^{8/5}\left(\frac{256}{5}\right)^{3/5} \simeq 14, \tag{3.12}$$

or, alternatively,

$$f\mathcal{M} \ll \frac{1}{\pi}\left(\frac{5}{256}\frac{8}{3\pi}\right)^{3/5} \simeq \frac{1}{37}. \tag{3.13}$$

For binary systems that will be observable by LIGO/VIRGO-like interferometers,

$$f\mathcal{M} = 6\times10^{-4}\frac{f}{100\,\mathrm{Hz}}\frac{\mathcal{M}}{1.2\,\mathrm{M}_\odot} \ll \frac{1}{37}; \tag{3.14}$$

consequently, the stationary phase approximation is a good one for our purposes. We thus have

$$\widetilde{m}(f) \simeq \begin{cases} \mathcal{A}\mathcal{M}^2\left[\frac{5\pi}{384}\right]^{1/2}(\pi f\mathcal{M})^{-7/6} & \\ \qquad\times\exp\left\{i\left[2\pi fT + \frac{3}{128}(\pi f\mathcal{M})^{-5/3} - \psi + \frac{\pi}{4}\right]\right\} & \text{for } f>0, \\ \widetilde{m}^*(-f) & \text{for } f<0. \end{cases} \tag{3.15}$$

C. The signal-to-noise ratio

Now suppose that we have analyzed the output $g(t)$ of an interferometer for the signal m and found that the likelihood function is maximized for the parameterization $\{\hat{\mathcal{A}}, \hat{\mathcal{M}}, \hat{\psi}, \hat{T}\}$. The SNR ρ^2 is then given by (*cf.* eqn. 2.4)

$$\begin{aligned}\rho^2 &= 2\left\langle m(\hat{\boldsymbol{\mu}}), m(\hat{\boldsymbol{\mu}})\right\rangle \\ &= \frac{5}{96\pi^{4/3}}\hat{\mathcal{A}}^2\hat{\mathcal{M}}^{5/3}f_{7/3},\end{aligned} \tag{3.16}$$

where, if we assume that we have access to $g(t)$ for all t,

$$f_{7/3} = \int_0^\infty df \, \left[f^{7/3} S_h(f) \right]^{-1} . \tag{3.17}$$

In practice, of course, data analysis is limited to a finite length sample of the interferometer output. During this limited interval, the signal "frequency" f (eqn. 3.5f) of an inspiralling binary system ranges from f_l to f_h. We assume that the minimum of $S_h(f)$ occurs in this interval and not too near the endpoints. Then, just as the slowly varying amplitude and frequency of m permitted us to estimate $\widetilde{m}(f)$ using the stationary phase approximation, so it allows us to approximate ρ^2 for a finite duration observation by replacing the lower and upper limits in the integral expression for $f_{7/3}$ (eqn. 3.18) by f_l and f_h. The lower bound f_l is determined by the duration of the data stream being analyzed while the upper bound f_h is determined by the coalescence of the binary components. We further assume that the $f_{7/3}$ does not change significantly as $f_h \to \infty$; thus, we have

$$f_{7/3} = \int_{f_l}^\infty df \, \left[f^{7/3} S_h(f) \right]^{-1} . \tag{3.18}$$

We discuss our choice of low-frequency cut-off f_l in §IV A 6 and again in §V D.

D. The covariance matrix

Turn now to the calculation of the covariance matrix $\mathcal{C}_{ij}$ (*cf.* eqn. 2.7b). Instead of a parameterization in terms of $\mathcal{A}$ and $\mathcal{M}$, it is more convenient to introduce η and ζ defined by

$$\widehat{\mathcal{A}}(1+\eta) \equiv \mathcal{A} \tag{3.19a}$$

$$\widehat{\mathcal{M}}(1+\zeta) \equiv \mathcal{M}, \tag{3.19b}$$

where $\widehat{\mathcal{A}}$ and $\widehat{\mathcal{M}}$ are the modes of the observed distribution of $\mathcal{A}$ and $\mathcal{M}$.

Given our expression for $\widetilde{m}(f)$, we can evaluate all of the elements of the symmetric matrix $\mathcal{C}_{ij}^{-1}$ in terms of the *frequency moments* $\overline{f}_\beta$ defined by

$$\overline{f}_\beta \equiv f_{7/3}^{-1} \int_{f_l}^\infty df \, \left[f^\beta S_h(f) \right]^{-1} . \tag{3.20}$$

To express $\mathcal{C}_{ij}$, only $\overline{f}_\beta$ for $\beta \in \{17/3,\ 4,\ 3,\ 7/3,\ 1/3\}$ are needed. In terms of these moments,

$$\mathcal{C}_{ij}^{-1} = \rho^2 \begin{pmatrix} 1 & \frac{5}{6} & 0 & 0 \\ & \frac{25}{36}\left[1 + \frac{9}{4096}\frac{\overline{f}_{17/3}}{\left(\pi\widehat{\mathcal{M}}\right)^{10/3}}\right] & \frac{5}{128}\frac{\overline{f}_4}{\left(\pi\widehat{\mathcal{M}}\right)^{5/3}} & -\frac{5\pi}{64}\frac{\overline{f}_3}{\left(\pi\widehat{\mathcal{M}}\right)^{5/3}} \\ & & 1 & -2\pi\overline{f}_{4/3} \\ & & & (2\pi)^2\overline{f}_{1/3} \end{pmatrix}, \tag{3.21}$$

where the indices are ordered η, ζ, ψ, and T. We have inverted equation 3.21 to find $\mathcal{C}_{ij}$ and so the variances and correlation coefficients describing the distributions of η, ζ, ψ, and T (*cf.* eqns. 2.18 and 2.19). The variances are

$$\sigma_\eta^2 = \frac{\sigma_{\mathcal{A}}^2}{\widehat{\mathcal{A}}^2}$$
$$= \left[1 + \frac{4096}{9\Delta}\left(\pi\widehat{\mathcal{M}}\right)^{10/3}\left(\overline{f}_{1/3} - \overline{f}_{4/3}^2\right)\right]\rho^{-2} \tag{3.22a}$$
$$\sigma_\zeta^2 = \frac{\sigma_{\mathcal{M}}^2}{\widehat{\mathcal{M}}^2}$$
$$= \frac{16384}{25\Delta\rho^2}\left(\overline{f}_{1/3} - \overline{f}_{4/3}^2\right)\left(\pi\widehat{\mathcal{M}}\right)^{10/3} \tag{3.22b}$$
$$\sigma_\psi^2 = \frac{\overline{f}_{17/3}\overline{f}_{1/3} - \overline{f}_3^2}{\Delta\rho^2} \tag{3.22c}$$
$$\sigma_T^2 = \frac{\overline{f}_{17/3} - \overline{f}_4^2}{4\pi^2\Delta\rho^2} \tag{3.22d}$$

and the correlation coefficients are

$$r_{\eta\zeta} = r_{\mathcal{A}\mathcal{M}}$$
$$= \frac{64\left(\overline{f}_{4/3}^2 - \overline{f}_{1/3}\right)\left(\pi\widehat{\mathcal{M}}\right)^{10/3}}{\left\{\left[9\Delta + 4096\left(\pi\widehat{\mathcal{M}}\right)^{10/3}\left(\overline{f}_{1/3} - \overline{f}_{4/3}^2\right)\right]\left(\overline{f}_{1/3} - \overline{f}_{4/3}^2\right)\left(\pi\widehat{\mathcal{M}}\right)^{10/3}\right\}^{1/2}}, \tag{3.23a}$$
$$r_{\eta\psi} = r_{\mathcal{A}\psi}$$
$$= \frac{64\left(\overline{f}_{1/3}\overline{f}_4 - \overline{f}_{4/3}\overline{f}_3\right)\left(\pi\widehat{\mathcal{M}}\right)^{5/3}}{\left\{\left[9\Delta + 4096\left(\pi\widehat{\mathcal{M}}\right)^{10/3}\left(\overline{f}_{1/3} - \overline{f}_{4/3}^2\right)\right]\left(\overline{f}_{17/3}\overline{f}_{1/3} - \overline{f}_3^2\right)\right\}^{1/2}}, \tag{3.23b}$$
$$r_{\eta T} = r_{\mathcal{A}T}$$
$$= \frac{64\left(\overline{f}_4\overline{f}_{4/3} - \overline{f}_3\right)\left(\pi\widehat{\mathcal{M}}\right)^{5/3}}{\left\{\left[9\Delta + 4096\left(\pi\widehat{\mathcal{M}}\right)^{10/3}\left(\overline{f}_{1/3} - \overline{f}_{4/3}^2\right)\right]\left(\overline{f}_{17/3} - \overline{f}_4^2\right)\right\}^{1/2}}, \tag{3.23c}$$
$$r_{\zeta\psi} = r_{\mathcal{M}\psi}$$
$$= \frac{\left(\overline{f}_{4/3}\overline{f}_3 - \overline{f}_{1/3}\overline{f}_4\right)}{\left[\left(\overline{f}_{1/3} - \overline{f}_{4/3}^2\right)\left(\overline{f}_{17/3}\overline{f}_{1/3} - \overline{f}_3^2\right)\right]^{1/2}}, \tag{3.23d}$$
$$r_{\zeta T} = r_{\mathcal{M}T}$$
$$= \frac{\overline{f}_3 - \overline{f}_4\overline{f}_{4/3}}{\left[\left(\overline{f}_{1/3} - \overline{f}_{4/3}^2\right)\left(\overline{f}_{17/3} - \overline{f}_4^2\right)\right]^{1/2}}, \tag{3.23e}$$
$$r_{\psi T} = \frac{\overline{f}_{17/3}\overline{f}_{4/3} - \overline{f}_4\overline{f}_3}{\left[\left(\overline{f}_{17/3}\overline{f}_{1/3} - \overline{f}_3^2\right)\left(\overline{f}_{17/3} - \overline{f}_4^2\right)\right]^{1/2}}, \tag{3.23f}$$

where

$$\Delta \equiv \left(\overline{f}_{1/3} - \overline{f}_{4/3}^2\right)\overline{f}_{17/3} - \overline{f}_{1/3}\overline{f}_4^2 + \left(2\overline{f}_4\overline{f}_{4/3} - \overline{f}_3\right)\overline{f}_3 > 0. \tag{3.24}$$

E. Properties of $\mathcal{A}$

Despite the fact that we cannot measure the orientation angles relating the interferometer to the source, we still need them in order to assess the interferometer's sensitivity. Recalling that

$$m = F_+ h_+ + F_\times h_\times, \tag{3.25}$$

we express F_+ and $F_\times$ according to the following convention:

1. Assume that the interferometer arms are the same length and that they meet in right angles.

2. Define a right-handed coordinate system with one interferometer arm along the x-axis and the other along the y-axis. Denote the unit vector in the direction of the x arm by $\mathbf{l}$ and the unit vector in the direction of the y arm by $\mathbf{m}$.

3. Let the position of a source in the sky be given by the polar angle θ and the azimuthal angle ϕ, and denote the unit vector pointing toward the source by $\mathbf{n}_S$ (*i.e.*, $-\mathbf{n}_I$).

4. The interferometer responds linearly to the radiation field $\mathbf{h}$, so its response m can be represented by a tensor $\mathbf{R}$ such that

$$m = \mathbf{R}\!:\!\mathbf{h}. \tag{3.26}$$

   For our interferometric detector

$$\mathbf{R} \equiv \frac{1}{2}\left(\mathbf{l}\otimes\mathbf{l} - \mathbf{m}\otimes\mathbf{m}\right). \tag{3.27}$$

5. Assume that axis $\mathbf{e}_x^R$ makes an angle ζ with the axis $\mathbf{l}$, *i.e.*,

$$\mathbf{e}_x^R = \mathbf{l}\cos\zeta + \mathbf{m}\sin\zeta. \tag{3.28}$$

With these conventions, the antenna patterns are given by [40]

$$\begin{aligned} F_+ &\equiv \mathbf{R}\!:\!\mathbf{e}_+ \\ &= \frac{1}{2}\cos 2\zeta\left(1+\cos^2\theta\right)\cos 2\phi - \sin 2\zeta\cos\theta\sin 2\phi \qquad (3.29a) \\ F_\times &= \mathbf{R}\!:\!\mathbf{e}_\times \\ &= \frac{1}{2}\sin 2\zeta\left(1+\cos^2\theta\right)\cos 2\phi + \cos 2\zeta\cos\theta\sin 2\phi \qquad (3.29b) \end{aligned}$$

and the amplitude $\mathcal{A}^2$ may be written

$$\mathcal{A}^2 = \frac{4}{{d_L}^2}\left[F_+^2\left(1+\cos^2 i\right)^2 + 4F_\times^2\cos^2 i\right]. \tag{3.30}$$

It is convenient to denote the angular dependence of $\mathcal{A}^2$ by Θ^2:

$$\Theta^2 = 4\left[F_+^2\left(1+\cos^2 i\right)^2 + 4F_\times^2\cos^2 i\right]. \tag{3.31}$$

The range of Θ^2 is $0 \leq \Theta^2 \leq 16$.

The SNR ρ^2 and covariance matrix $\mathcal{C}_{ij}$ (eqns. 2.4 and 2.7b) both depend on $\mathcal{A}^2$, which is in turn a function of the (unknown) relative orientation of the source and interferometer through Θ^2. In order to evaluate the expected ρ^2 (or the expected $\mathcal{C}_{ij}$) of a source at a given distance d_L we need to know some properties of the probability distribution of Θ^2.

Since Θ^2 depends on the angles θ, ϕ, i, and ζ (*cf.* eqn. 3.31), the *a priori* distribution of Θ^2 depends on the *a priori* distribution of these angles. These distributions are all known: in particular, $\cos\theta$ and $\cos i$ are uniformly distributed over the range $[-1,1]$ and ϕ and ζ are uniformly distributed over the range $[0,2\pi)$. Making use of the definitions of F_+ and $F_\times$ (eqns. 3.29a and 3.29b), we find that the mean square of Θ is

$$\overline{\Theta^2} = \frac{64}{25}. \tag{3.32}$$

The distribution of Θ^2 is not symmetric, however: in fact, its mode is zero and larger values of Θ^2 are much less likely to occur than smaller ones. We have determined the cumulative distribution function of Θ^2 using a Monte Carlo analysis; we give the percentiles of the distribution in table I. In performing these calculations, we used Knuth's portable random number generator [43] as implemented by Press *et al.* [44] (*i.e.*, their RAN3). The results in table I are based on a sample of 10^7 points in the $\{\cos\theta,\ \cos i,\ \phi,\ \zeta\}$ parameter space. The corresponding values of Θ^2 were sorted into bins and the reported percentiles are the rounded bin centers.

Note from table I that significantly more than half (*i.e.*, approximately 65%) of the inspiralling binary systems will have Θ^2 less than $\overline{\Theta^2}$. The skew of the distribution toward smaller Θ^2 plays a significant role when we estimate the range of the interferometer (*cf.* §V B).

IV. APPLICATION TO LIGO

In §III we found expressions for the SNR, the variance, and correlation coefficients corresponding to the detection of a signal characterized by $\hat{\mathcal{A}}$, $\hat{\mathcal{M}}$, $\hat{\psi}$, and $\hat{T}$. In this section we join those expressions with the design characteristics of LIGO/VIRGO-like interferometers to obtain estimates for the sensitivity of a realistic interferometric detector to inspiralling binaries.

A. Noise and the LIGO interferometers

The characteristic of the interferometers enter our analysis solely through the strain noise PSD $S_h(f)$. The dominant contributions to $S_h(f)$ for the interferometer configurations that will be used to search for inspiralling binaries are from seismic, thermal, and photon shot noise. In this subsection we summarize these contributions to the overall noise PSD that we use in our calculations.

1. Photon shot noise

At high frequencies $S_h(f)$ is dominated by photon shot noise. The shot noise depends on the interferometer arm lengths, laser power and wavelength, mirror reflectivities and configuration in a complicated fashion. In all of our calculations we have assumed that LIGO/VIRGO will be equipped with Fabrey-Perot cavity interferometers, and we have used the analysis of Krolak, Lobo, and Meers [28, *cf.* their eqns. 2.11-22] to describe the photon shot noise. This analysis is general enough to encompass non-recycling, standard recycling, and dual recycling interferometers. Except in §IV B we always assume that the instrumentation makes use of standard recycling techniques. For standard recycling, the photon shot noise is given approximately by Thorne [40, eqn. 117c] or Krolak, Lobo, and Meers [28, eqn. 3.5]

$$S_h^{\rm shot}(f) = \frac{\hbar\lambda}{\eta I_0}\frac{A^2}{L} f_c \left[1 + \left(\frac{f}{f_c}\right)^2\right], \tag{4.1}$$

where A^2 describes the mirror losses, I_0 is the laser power, η is the quantum efficiency of the photo-detector, λ is the laser wavelength, L is the length of interferometer arms, and f_c is the recycling "knee" frequency.

The simplest way in which the observer can change the noise characteristics of the LIGO/VIRGO instrumentation is by changing the recycling knee frequency f_c. The general trend is that, as the recycling frequency increases the bandwidth increases while the sensitivity across the bandwidth decreases [40, fig. 9.13].

2. Thermal noise

At lower frequencies, off-resonance thermal excitations of the test mass suspensions and internal modes of the pendulum masses either dominate or provide important contributions to the noise. We approximate the suspension noise by focusing only on the pendulum mode (ignoring both torsional and violin modes). If the dissipative force in the pendulum suspension is due to friction, then the strain PSD of a single test mass m with resonant frequency f_0 and quality factor Q_0 at temperature T is given by

$$S_h^{\rm pend}(f) = \frac{k_{\rm B} T f_0}{2\pi^3 m Q_0 L^2 \left[(f^2 - f_0^2)^2 + (f f_0/Q_0)^2\right]} \tag{4.2}$$

(note that we use T for both the temperature and the Newtonian "moment of coalescence;" nevertheless, the meaning of the symbol in any given context should be clear). Each arm of the interferometer has a pendulum degree of freedom at each end and the noise from each degree of freedom is independent; thus, the total noise PSD is a factor of four greater than this (note that Dhurandhar, Krolak and Lobo [22, eqn. 2.10] neglect this factor of four in their analysis and have several typographical errors in their formulae). The total thermal suspension noise PSD is given by

$$S_h^{\rm susp}(f) = 4 S_h^{\rm pend}(f). \tag{4.3}$$

The primary dissipative force acting on the pendulum may not be friction, however: it has been suggested [23] that the dissipation is due instead to a phase lag between the stress and the strain in the pendulum suspension. If this is the case, then the noise PSD is different than that given above. This is not an issue for the initial interferometers, but will be for the advanced ones [13]. The nature of the dissipation is far from settled, and in the absence of a consensus we have used the form given in equation 4.3.

Off-resonance thermal excitations of the vibrational modes of the test masses will also be a significant source of noise in the LIGO/VIRGO interferometers. Here we consider only the fundamental vibrational mode of each test mass. The contribution to the noise PSD has the same form as the thermal suspension noise $S_h^{\rm susp}(f)$ (and is subject to the same controversy), only now the resonant frequency and oscillator quality that enter are those of the test masses:

$$S_h^{\rm int}(f) = \frac{2k_{\rm B}T f_{\rm int}}{\pi^3 m Q_{\rm int} L^2 \left[(f^2 - f_{\rm int}^2)^2 + (f f_{\rm int}/Q_{\rm int})^2 \right]}. \tag{4.4}$$

3. Seismic noise

Seismic noise will dominate $S_h(f)$ at low frequencies. Saulson [45] has surveyed the literature on the seismic displacement noise PSD $S_x(f)$ and finds that it is roughly proportional to f^{-4} in the range $1/10\,{\rm Hz} \lesssim f \lesssim 10\,{\rm Hz}$. Consequently, if the LIGO/VIRGO test mass suspensions were coupled directly to the Earth, then

$$S_h^{\rm seismic}(f) = \frac{S_0' f^{-4}}{(f_0^2 - f^2)^2 + (f f_0/Q_0)^2} \tag{4.5}$$

where f_0 is the pendulum mode frequency, Q_0 is pendulum quality, and S_0' is a proportionality constant with units of $\rm Hz^7$. Note that at frequencies above the pendulum frequency f_0 the seismic strain noise is proportional to f^{-8} while below f_0 is is proportional to f^{-4}.

In the actual LIGO/VIRGO interferometers, the pendulum suspensions will be isolated from the Earth by a mechanical circuit that is a series of several highly damped oscillators [46,47]. Each oscillator in this series circuit will introduce four poles in the strain noise PSD near the pendulum frequency; consequently, the actual seismic noise contribution will be much steeper than f^{-8} at frequencies greater than f_0 and much more complicated near the resonant frequencies of the mechanical circuit. It is proposed that seismic isolation in the initial interferometers be provided by a five stage circuit (where the final stage of isolation is the pendulum suspension itself) [46, §V 3 b and appendix D]; consequently, for frequencies much greater than f_0 the seismic strain noise PSD is expected to be proportional to f^{-24}. Nearer the resonant frequencies of the isolation circuit the dependence is quite complicated as the poles in the response function are not at zero frequency, but at complex frequencies with real parts near 1 Hz. The strain noise PSD below the resonant frequencies of the isolation circuit remains proportional to the displacement noise PSD $S_x(f)$.

In our calculations we use the following crude estimate for the seismic strain noise PSD:

$$S_h^{\rm seismic}(f) = \frac{S_0 f^{-4}}{(f^2 - f_0^2)^{10}}. \tag{4.6}$$

The proportionality constant S_0 has units of Hz^{23}. This estimate scales correctly with frequency above and below f_0, though it fails near f_0. This failure is unimportant since (except in §V D) we assume that $f_l > f_0$ (the choice of cut-off f_l is discussed in §IV A 6).

The amplitude of the noise (as reflected by the proportionality constant S_0) depends on the detailed nature of the seismic isolation circuit and the properties of the seismic displacement noise at the interferometer site. The LIGO design goals for the initial and advanced interferometers are [46]

$$S_h^{\mathrm{seismic}}(40\,\mathrm{Hz}) = S_h^{\mathrm{susp}}(40\,\mathrm{Hz}) + S_h^{\mathrm{int}}(40\,\mathrm{Hz}) \qquad \text{(initial interferometers)} \tag{4.7a}$$

$$S_h^{\mathrm{seismic}}(10\,\mathrm{Hz}) = S_h^{\mathrm{susp}}(10\,\mathrm{Hz}) + S_h^{\mathrm{int}}(10\,\mathrm{Hz}) \qquad \text{(advanced interferometers).} \tag{4.7b}$$

We fix S_0 by these relationships. Where we discuss the advanced LIGO *detectors*, we use the same condition on the seismic noise as for the advanced interferometers.

4. Quantum noise

In addition to the primary noise sources discussed above, we have also included a contribution whose origin is quantum mechanical and rooted in the Heisenberg uncertainty principle. When we observe a signal of frequency f in an interferometer, we are measuring the periodic motion of the end-masses at that frequency. Since the motion is periodic, this is equivalent to a simultaneous measurement of the momentum and localization of the end masses, and the precision with which we can make this measurement is subject to the usual quantum mechanical limits. In our calculations, we use the form of the quantum noise given by Thorne [40, eqn. 121]:

$$S_h^{\mathrm{quant}}(f) = \frac{8\hbar}{m\,(2\pi f)^2\,L^2}, \tag{4.8}$$

where m is the mass of the LIGO pendulum bobs.

5. Noise source summary

In table II we give the instrument characteristics we have assumed in our calculations. Two sets of values are given, corresponding to estimates for LIGO initial and advanced instrumentation. These estimates have been culled from the literature [1,2], the LIGO proposal [46], and personal communication with members of the LIGO project [13,48]. In terms of the noise sources discussed in the previous subsections, the noise PSD $S_h(f)$ we use in our calculations is

$$\begin{aligned} S_h(f) = {} & S_h^{\mathrm{shot}}(f) + S_h^{\mathrm{int}}(f) + S_h^{\mathrm{susp}}(f) \\ & + S_h^{\mathrm{seismic}}(f) + S_h^{\mathrm{quant}}(f). \end{aligned} \tag{4.9}$$

As a companion to table II and as a graphical illustration of how all of the noise sources discussed above act in concert to determine an interferometer's noise characteristics, we show our approximation to the anticipated $S_h(f)$ for both the initial (fig. 1) and advanced (fig. 2)

instrumentation. The contributions to $S_h(f)$ from each of the influences discussed above are shown as dashed lines and $S_h(f)$ is shown as a solid line. Both figures show interferometers configured to operate in standard recycling mode. In figure 1, corresponding to the initial interferometers, the recycling frequency f_c is 300 Hz, while in figure 2 (corresponding to the advanced interferometer design) it is 100 Hz.

6. Choosing the low frequency cut-off f_l

The elements of the covariance matrix $\mathcal{C}_{ij}$ depend on the moments $f_{7/3}$, $\overline{f}_{17/3}$, $\overline{f}_4$, $\overline{f}_3$, $\overline{f}_{4/3}$, and $\overline{f}_{1/3}$. In turn, these depend on $S_h(f)$ and the low frequency cut-off f_l (see eqns. 3.18 and 3.20). Our calculations of these moments have assumed a low frequency cut-off of 10 Hz, corresponding to the last several minutes in the inspiral of a binary neutron star system. In table III we give the frequency moments $f_{7/3}$, $\overline{f}_{17/3}$, $\overline{f}_4$, $\overline{f}_3$, $\overline{f}_{4/3}$, and $\overline{f}_{1/3}$ for two cases of interest.

7. The LIGO detector

The two LIGO interferometers, though separated by several thousand miles, share nearly the same orientation in space: the planes defined by the detector arms are nearly parallel, and the arms themselves are nearly parallel. Consequently the network acts like a single interferometer of greater sensitivity than either of its components. If the noise in the two component interferometers of the LIGO detector is uncorrelated and described by $S_h^{(0)}(f)$, then the effective PSD of the more sensitive single interferometer is $S_h(f) = S_h^{(0)}(f)/2$. Consequently, the effective PSD for the LIGO detector in the limit that the interferometers share the same orientation is also given by figure 2, but with the scale reduced by a factor of $2^{-1/2}$. In making this approximation we are ignoring the differences in arrival time of the gravitational radiation signal at the two interferometers. In the following sections when we refer to the LIGO *detector* (as opposed to a LIGO/VIRGO-like interferometer) we are actually referring to a single interferometer whose noise PSD is 1/2 that of the advanced interferometer design.

B. Signal-to-noise ratio

As discussed in §II B, we decide whether or not a signal is present in the output of the detector by comparing the likelihood ratio Λ to a pre-determined threshold. In this regard, the SNR ρ^2 is an acceptable surrogate for Λ; *i.e.,* we can choose a threshold ρ_0^2 (which may be a function of $\widehat{\boldsymbol{\mu}}$) to compare with ρ^2. Then, if $\rho^2 \geq \rho_0^2$ we assert the presence of a signal while if $\rho^2 < \rho_0^2$ we conclude that the detector output is only noise. The choice of threshold is a delicate matter: on the one hand we want a high threshold to minimize the probability that we misidentify noise as signal; on the other hand, we want a low threshold to minimize the probability that we misidentify a real signal as noise. We will consider the proper choice of the threshold ρ_0^2 in a later paper; now, however, we assume only that the threshold depends weakly on the detection strategy and $\boldsymbol{\mu}$.

The amplitude SNR ρ may be expressed

$$\rho = 8 \left(\frac{\mathcal{M}}{1.2\,\mathrm{M}_\odot} \right)^{5/6} \left(\frac{\Theta}{\Theta_{50\%}} \right) F_{7/3} \times \begin{cases} (17.0\,\mathrm{Mpc}/d_L) & \text{initial interferometers} \\ (308.\,\mathrm{Mpc}/d_L) & \text{advanced interferometers} \\ (436.\,\mathrm{Mpc}/d_L) & \text{advanced LIGO detector} \end{cases} \tag{4.10}$$

where

$$F_{7/3}(f_c, f_l) \equiv \left[\frac{f_{7/3}(f_c, f_l)}{f_{7/3}(100\,\mathrm{Hz}, 10\,\mathrm{Hz})} \right]^{1/2} \tag{4.11a}$$

$$= \begin{cases} \left(f_{7/3} / 5.331 \times 10^{42}\,\mathrm{Hz}^{-1/3} \right)^{1/2} & \text{initial interferometers} \\ \left(f_{7/3} / 1.747 \times 10^{45}\,\mathrm{Hz}^{-1/3} \right)^{1/2} & \text{advanced interferometers} \\ \left(f_{7/3} / 3.493 \times 10^{45}\,\mathrm{Hz}^{-1/3} \right)^{1/2} & \text{advanced LIGO detector} \end{cases} \tag{4.11b}$$

In figure 3 we show $F_{7/3}$ for both the initial and advanced LIGO instrumentation. Two curves are shown: one for the initial interferometers and one for the advanced interferometers. Each curve assumes a low-frequency cutoff f_l of 10 Hz (corresponding to the last several minutes of binary neutron star inspiral). For the advanced instrumentation the detection strategy that maximizes ρ has $f_c = 100$ Hz (where $F_{7/3} = 1$), while for the initial instrumentation $f_c = 300$ Hz (where $F_{7/3} = 1.3$). These correspond to the choice of f_c in figures 1 and 2 showing the detailed breakdown of $S_h(f)$ for the initial and advanced interferometers.

Now consider the case of resonant dual recycling [19,21,24]. The photon shot noise in an interferometer operating in a resonant dual recycling mode is proportional to (*cf.* [28] eqn. 3.7 but note that their approximate expression has several errors; see also [19,24])

$$S_h^{\mathrm{dual}}(f) \propto \left[1 + \left(\frac{f - f_n}{\Delta f} \right)^2 \right], \tag{4.12}$$

where Δf and f_n depend on the reflectivities of certain mirrors in the experimental apparatus. This shot noise PSD is large except in a narrow band about f_n where it is very small. The bandwidth Δf and the central frequency f_n of this "notch" can be adjusted, and the size of S_h^{dual} in and out of the notch will vary depending on the f and Δf. In comparison, an interferometer operating in standard recycling mode has a nearly constant shot noise PSD for frequencies below the knee frequency f_c, with the noise PSD increasing as f^2 for frequencies greater that f_c (*cf.* eqn. 4.1 and figs. 1 and 2). For $|f - f_n| \lesssim \Delta f$, dual recycling cuts a notch in S_h^{dual}. Elsewhere, S_h^{shot} is lower than that for dual recycling (assuming $f_0 \simeq f_c$). On the basis of numerical investigations of the interferometer response and the waveform of inspiralling binary systems, Krolak, Lobo, and Meers [28] suggested that dual recycling with $f_n = 100$ Hz and $\Delta f \simeq 6$ Hz is superior to standard recycling for the observation of binary systems. Their analysis assumed that $S_h(f)$ is infinite below 100 Hz and that only photon shot noise is important above 100 Hz: in particular, they did not consider the noise owing to the thermal excitations of the test mass vibrational modes (*cf.* §IV A 2). When $S_h^{\mathrm{int}}(f)$

is included in the analysis, then the advantage of dual recycling in this regime is lost: the notch is "filled in" by the thermal noise almost to the level of standard recycling photon shot noise (*cf.* their fig. 5 and our figs. 1 or 2), and everywhere else the noise is much greater than is the case for an interferometer operated in standard recycling mode.

Dual recycling may still be useful at much higher frequencies where the photon shot noise is a standard recycling configuration is much larger than the thermal noise (*e.g.*, 1.5 KHz). Observations at such high frequencies may prove useful for detecting the actual coalescence event [42].

V. ASTROPHYSICAL IMPLICATIONS

A. Source rate

Chernoff and Finn [16] have shown that the observed differential rate $d\dot{N}/d\mathcal{M}d\mathcal{A}$ of inspiralling binary systems depends on the cosmological model; consequently, it can be used to determine the Hubble constant H, the deceleration parameter q, and otherwise distinguish between cosmologies. Here we are interested in the total rate of observed binary inspiral as an estimate of the sensitivity of an interferometer, and in this subsection we estimate that rate ignoring cosmological effects. We refer the reader interested in a rate calculation consistent with an expanding universe and taking into account evolution of the binary population and distribution of $\mathcal{M}$ in binaries to Chernoff and Finn [16].

Assume that the rate density (number per unit co-moving cosmological volume per unit time) of inspiralling neutron-star binary systems is a constant $\dot{\mathcal{N}}$ and that the variation in neutron star masses is small so that $\mathcal{M}$ is approximately equal to $1.2\,\mathrm{M}_\odot$ (corresponding to two $1.4\,\mathrm{M}_\odot$ neutron stars). The expected total rate $\dot{N}$ of systems whose SNR ρ^2 is greater than ρ_0^2 is

$$\begin{aligned}
\dot{N} &= \int_0^\infty dr\, 4\pi \dot{\mathcal{N}} r^2 P\left[\rho^2(r) > \rho_0^2\right] \\
&= \int_0^\infty dr\, 4\pi \dot{\mathcal{N}} r^2 P\left(\Theta^2 > \frac{r^2}{r_0^2}\right) \\
&= 4\pi \dot{\mathcal{N}} r_0^3 \int_0^\infty dx\, x^2 P\left(\Theta^2 > x^2\right) \qquad (5.1a) \\
&\equiv \frac{4\pi}{3} \dot{\mathcal{N}} \mathcal{R}^3, \qquad (5.1b)
\end{aligned}$$

where

$$P\left(\Theta^2 > x^2\right) \equiv \left(\text{The probability that } \Theta^2 \text{ is greater than } x^2\right) \qquad (5.2a)$$

$$\begin{aligned}
r_0 &\equiv \left(\frac{5\mathcal{M}^{5/3} f_{7/3}}{96\pi^{4/3}\rho_0^2}\right)^{1/2} \\
&= \left(\frac{\mathcal{M}}{1.2\,\mathrm{M}_\odot}\right)^{5/6} \left(\frac{8}{\rho_0}\right) F_{7/3}
\end{aligned}$$

$$\times \begin{cases} 13.0\,\mathrm{Mpc} & \text{initial interferometer} \\ 236.\,\mathrm{Mpc} & \text{advanced interferometer} \\ 334.\,\mathrm{Mpc} & \text{advanced LIGO detector,} \end{cases} \tag{5.2b}$$

$$\mathcal{R} \equiv r_0 \left[3 \int_0^\infty dx\, x^2 P\left(\Theta^2 > x^2\right) \right]^{1/3} \tag{5.2c}$$

[recall that we have ignored cosmological effects (*cf.* Chernoff and Finn [16]) in eqn. 5.1a]. Using the cumulative distribution function for Θ^2 (*cf.* §III E and tbl. I), we find that

$$\int_0^\infty dx\, x^2 P\left(\Theta^2 > x^2\right) = 1.84; \tag{5.3}$$

hence,

$$\mathcal{R} = \left(\frac{\mathcal{M}}{1.2\,\mathrm{M}_\odot}\right)^{5/6} \left(\frac{8}{\rho_0}\right) F_{7/3} \times \begin{cases} 23.0\,\mathrm{Mpc} & \text{initial interferometer} \\ 417.\,\mathrm{Mpc} & \text{advanced interferometer} \\ 589.\,\mathrm{Mpc} & \text{advanced LIGO detector.} \end{cases} \tag{5.4}$$

Phinney [4] has given estimates for the number density of sources per unit time ($\dot{\mathcal{N}}$) based on observational and theoretical arguments. These estimates range from an ultra-conservative $6 \times 10^{-10}\,\mathrm{Mpc}^{-3}\mathrm{yr}^{-1}$, to a conservative $8 \times 10^{-8}\,\mathrm{Mpc}^{-3}\mathrm{yr}^{-1}$, to an upper limit of $6 \times 10^{-5}\,\mathrm{Mpc}^{-3}\mathrm{yr}^{-1}$. They are based on the statistics of local populations of binary pulsars and type Ib supernovae, and the large range reflects both the small size of the local sample, uncertainties in our understanding in the evolution of binary systems, and uncertainties in the selection effects at work in determining the fraction of the local systems we have direct knowledge of. If we take the typical threshold ρ_0 to be 8, then we find that expected rate of detections of inspiralling binary systems is

$$\dot{N} \simeq \frac{\dot{\mathcal{N}}}{8 \times 10^{-8}\,\mathrm{Mpc}^{-3}\mathrm{yr}^{-1}} \left(\frac{\mathcal{M}}{1.2\mathrm{M}_\odot}\right)^{5/2} \left(\frac{8}{\rho_0}\right)^3 F_{7/3}^3 \times \begin{cases} 4.1 \times 10^{-3}\,\mathrm{yr}^{-1} & \text{initial interferometer} \\ 24.\,\mathrm{yr}^{-1} & \text{advanced interferomter} \\ 69.\,\mathrm{yr}^{-1} & \text{advanced LIGO detector.} \end{cases} \tag{5.5}$$

As commented earlier, to maximize the rate at which binaries are detected we need to choose f_c in order to maximize $F_{7/3}$.

For a binary system consisting of a 10 $\mathrm{M}_\odot$ black hole and a neutron star, $\mathcal{M} \simeq 3$, and for a binary system consisting of two 10 $\mathrm{M}_\odot$ black holes, $\mathcal{M} \simeq 9$ (recall that we are neglecting cosmological effects). Consequently, for these neutron-star/black-hole (black-hole/black-hole) binaries $\mathcal{R}_{90\%} \simeq 2$ Gpc (5 Gpc) for the advanced LIGO detector. The situation for determining the rate at which such systems will be detected is a bit more complicated. Phinney argues that black-hole/black-hole and black-hole/neutron-star binaries form at rates comparable to the neutron-star/neutron-star merger rate; however, the fraction which merge depends on the model dependent details that vary greatly [4], so no reliable estimate of the coalescence rate is available for use with eqn. 5.5.

B. Range

An important measure of the sensitivity of a LIGO/VIRGO-like interferometer is its "range," *i.e.*, the distance to which sources can be observed. The definition of the range is subtle. Not all inspiralling binaries within, *e.g.*, a distance $\mathcal{R}$ will be identified as such: for some, Θ will be less than $\mathcal{R}/r_0$, the corresponding SNR ρ^2 will be less than the threshold ρ_0^2, and the signal will be dismissed as noise. Similarly, not all inspiralling binaries outside a distance $\mathcal{R}$ will fail to be identified by the interferometer: for some Θ will be *greater* than $\mathcal{R}/r_0$, the SNR ρ^2 will be greater than ρ_0^2, and the signal will be identified as coming from a binary system. Since the range is a slippery concept, we define a range *function* $\mathcal{R}_\gamma$ such that a fraction γ of the observable sources fall within the distance $\mathcal{R}_\gamma$:

$$\gamma = \frac{\int_0^{\mathcal{R}_\gamma/r_0} dx\, x^2 P\left(\Theta^2 > x^2\right)}{\int_0^{\infty} dx\, x^2 P\left(\Theta^2 > x^2\right)}. \tag{5.6}$$

The quantity

$$\frac{\int_0^{z} dx\, x^2 P\left(\Theta^2 > x^2\right)}{\int_0^{\infty} dx\, x^2 P\left(\Theta^2 > x^2\right)} \tag{5.7}$$

is tabulated in the third column of table I, and we show γ as a function of $\mathcal{R}_\gamma/\mathcal{R}$ in figure 4. Note that

$$\mathcal{R}_{90\%} = \left(\frac{\mathcal{M}}{1.2\,\mathrm{M}_\odot}\right)^{5/6} \left(\frac{8}{\rho_0}\right) F_{7/3} \times \begin{cases} 37.2\,\mathrm{Mpc} & \text{initial interferometer} \\ 673.\,\mathrm{Mpc} & \text{advanced interferometer} \\ 952.\,\mathrm{Mpc} & \text{advanced LIGO detector,} \end{cases} \tag{5.8}$$

i.e., *for the advanced LIGO detector approximately 7 sources per year will be observed whose distance is greater than* 950, Mpc. Like the rate, the range is sensitive to the detection strategy so that if we wish to maximize the sensitivity of the interferometer to either we need to choose a detection strategy that maximizes $F_{7/3}$.

C. Standard deviation and correlation coefficients

First consider the measurement of $\mathcal{A}$. For all $\mathcal{M}$ and f_c relevant for both the initial and advanced LIGO/VIRGO-like interferometers, the fractional standard deviation σ_η (*cf.* 3.22a) of the waveform amplitude $\mathcal{A}$ is ρ^{-1}; consequently, *the maximum fractional one-sigma uncertainty in the determination of* $\mathcal{A}$ *is*

$$\frac{\sigma_{\mathcal{A}}}{\widehat{\mathcal{A}}} = 0.125 \frac{8}{\rho_0} \tag{5.9}$$

for both the initial and advanced interferometers. Additionally, the correlation coefficients $r_{\mathcal{A}i}$ all have magnitude less than 10^{-4}, indicating that $\mathcal{A}$ is statistically independent of $\mathcal{M}$.

ψ and T (*i.e.*, the random errors in measurements of $\mathcal{A}$ owing to detector noise are not correlated with the corresponding errors in the measurement of $\mathcal{M}$, ψ, or T).

Now turn to the measurement of $\mathcal{M}$. Before discussing the exact results obtained with equation 3.22b, we give a heuristic derivation of the precision with which $\mathcal{M}$ can be determined. Recall that the phase Φ of the gravitational wave signal is given by

$$\tilde{\Phi} = -2\left(\frac{\tilde{T}-t}{5\widetilde{\mathcal{M}}}\right)^{5/8} . \tag{5.10}$$

The observation encompasses approximately the last ten minutes in the life of the binary system, during which time the phase advances by

$$\Delta\tilde{\Phi} = 7.4\times 10^4 \left(\frac{\Delta t}{10\,\mathrm{m}}\frac{1.2\,\mathrm{M}_\odot}{\widetilde{\mathcal{M}}}\right)^{5/8} \text{rad.} \tag{5.11}$$

The argument of the exponential in the odds ratio (eqn. 2.3d) is

$$2\left\langle n, m(\boldsymbol{\mu})\right\rangle + 2\left\langle m(\tilde{\boldsymbol{\mu}}), m(\boldsymbol{\mu})\right\rangle - \left\langle m(\boldsymbol{\mu}), m(\boldsymbol{\mu})\right\rangle . \tag{5.12}$$

The contribution owing to the term $2\left\langle m(\tilde{\boldsymbol{\mu}}), m(\boldsymbol{\mu})\right\rangle$ is much greater than that owing to the noise; consequently, to a good approximation the odds ratio will be maximized where this quantity is maximized. Ignoring the frequency dependence of $S_h(f)$ the term $\left\langle m(\tilde{\boldsymbol{\mu}}), m(\boldsymbol{\mu})\right\rangle$ is the correlation between two sinusoidal functions of the phase, and is large only as long as the advance in phase of $m(\boldsymbol{\mu})$ is within approximately π radians of the advance in phase of $m(\tilde{\boldsymbol{\mu}})$ over the course of the observation. Since $\Delta\Phi$ depends only on $\mathcal{M}$, we have $\pi \gtrsim |\Delta\tilde{\Phi} - \Delta\Phi|$ or

$$\begin{aligned}\frac{\delta\mathcal{M}}{\mathcal{M}} &\lesssim \frac{4\pi}{5}\left(\frac{\widetilde{\mathcal{M}}}{\Delta t}\right)^{5/8} \\ &\lesssim 10^{-4}\left(\frac{\widetilde{\mathcal{M}}}{1.2\,\mathrm{M}_\odot}\frac{10\,\mathrm{m}}{\Delta t}\right)^{5/8} ,\end{aligned} \tag{5.13}$$

where $\delta\mathcal{M}$ is $\widetilde{\mathcal{M}} - \mathcal{M}$.

Return now to consider the exact results. Equation 3.22b gives the fractional standard deviation $\sigma_{\mathcal{M}}/\widehat{\mathcal{M}}$ in terms of the frequency moments $\overline{f}_\beta$ and ρ:

$$\begin{aligned}\frac{\sigma_{\mathcal{M}}}{\widehat{\mathcal{M}}} &= \left(\frac{\mathcal{M}}{1.2\,\mathrm{M}_\odot}\right)^{5/3}\left(\frac{8}{\rho}\right)\Sigma_{\mathcal{M}} \\ &\quad\times\begin{cases} 2.08\times 10^{-4} & \text{initial interferometer,} \\ 2.20\times 10^{-5} & \text{advanced interferometer}\end{cases}\end{aligned} \tag{5.14}$$

where

$$\Sigma_{\mathcal{M}} = \left[\left(\frac{\overline{f}_{1/3}-\overline{f}_{4/3}^2}{\Delta}\right) \Big/ \left(\frac{\overline{f}_{1/3}-\overline{f}_{4/3}^2}{\Delta}\right)\Bigg|_{f_c=100\,\mathrm{Hz}, f_l=10\,\mathrm{Hz}}\right]^{1/2} . \tag{5.15}$$

Given a threshold ρ_0 such that $\rho \geq \rho_0$ for all observed sources, equations 5.14 and 5.15 give the maximum fractional standard deviation in the measurement $\mathcal{M}$ for any binary system observed with LIGO/VIRGO-like interferometers — a phenomenal precision. In interpreting eqn. 5.14, note that $\sigma_{\mathcal{M}}/\widehat{\mathcal{M}}$ is inversely proportional to ρ, and recall that the SNR ρ of a binary system observed in an interferometer of the advanced design is approximately 26 times greater than the SNR of the same binary observed in a detector of the initial design (*cf.* eqn. 4.10). The results for the advanced LIGO detectors are identical to those for the advanced interferometers, except that the amplitude SNR ρ for a binary observed in the advanced detector is $2^{1/2}$ greater than that for the same binary observed in a single advanced interferometer.

In figure 5 we show $\Sigma_{\mathcal{M}}$ for both the initial and advanced interferometers. For the advanced interferometer the total variation of $\Sigma_{\mathcal{M}}$ is approximately 20% as f_c ranges from 50 Hz to 1 KHz, while for the initial interferometer the variation is approximately 15%. The optimum recycling frequency for measurement of $\mathcal{M}$ is that which minimizes Σ_M, and we see that this is very different than the choice which maximizes the number of binaries observed (*cf.* §IV B and fig. 3): in fact, the optimal choice of f_c for the detection of binaries (in either the initial or advanced interferometers) is close to the *worst* possible choice of f_c for the precise measurement of $\mathcal{M}$.

As we have pointed out, with observations in a single gravitational wave interferometer the location of the source on the sky cannot be determined. If, as has been suggested, some coalescing binaries result in γ-ray bursts [49,5], then burst observations may be used to localize the binary system in the sky. The identification between a gravitational wave burst from orbital decay (which takes place before actual coalescence of the binary components) and a γ-ray burst (which takes place at the time of coalescence) depends on the accuracy with which we can measure the time of arrival of the γ-ray burst and the "moment of coalescence" T: in all events, T will be within seconds of the actual moment of neutron star disruption and the emission of the γ-ray burst. Consequently, we need to know T, the rate of detected binary coalescence, and the rate of γ-ray bursts (the latter both assumed to be Poisson distributed in time) in order to evaluate the probability that a correlation in time between a γ-ray burst and a gravitational wave burst is coincidental. The accuracy with which we can determine T is given by σ_T (*cf.* 3.22d):

$$\sigma_T = \left(\frac{8}{\rho}\right) \Sigma_T \times \begin{cases} 1.54 \times 10^{-4}\,\mathrm{s} & \text{initial interferometer,} \\ 3.00 \times 10^{-4}\,\mathrm{s} & \text{advanced interferometer,} \end{cases} \tag{5.16}$$

where

$$\Sigma_T = \left[\left(\frac{\overline{f}_{17/3} - \overline{f}_4^2}{\Delta} \right) \Big/ \left(\frac{\overline{f}_{17/3} - \overline{f}_4^2}{\Delta} \right) \Bigg|_{f_c = 100\,\mathrm{Hz}, f_l = 10\,\mathrm{Hz}} \right]^{1/2} . \tag{5.17}$$

The results for the advanced LIGO detector are the same as those for a single advanced interferometer. The factor Σ_T varies by approximately a factor of 2.5 over the range $50\,\mathrm{Hz} < f_c < 1000\,\mathrm{Hz}$, and is shown (for both the initial and advanced interferometers) in figure 6.

Again, the optimal interferometer configuration for precision measurements of T is very different than that for detection of inspiralling binaries.

The parameter ψ depends on the orientation of the source and the detector and the phase of the binary systems orbit at $t = 0$. For completeness, we also give the precision with which ψ can be measured:

$$\sigma_\psi = \left(\frac{8}{\rho}\right) \Sigma_\psi \times \begin{cases} 0.257\,\text{rads} & \text{initial interferometer,} \\ 0.338\,\text{rads} & \text{advanced interferometer,} \end{cases} \tag{5.18}$$

where

$$\Sigma_\psi \equiv \left[\left(\frac{\overline{f}_{17/3} - \overline{f}_4^2}{\Delta} \right) / \left(\frac{\overline{f}_{17/3} - \overline{f}_4^2}{\Delta} \right) \Bigg|_{f_c=100\,\text{Hz}, f_l=10\,\text{Hz}} \right]^{1/2} . \tag{5.19}$$

The results for an advanced detector are the same as those for a single advanced interferometer.

The correlation coefficients $r_{\mathcal{M}\psi}$, $r_{\mathcal{M}T}$, and $r_{\psi T}$ are nearly independent of f_c for both the initial and advanced LIGO-like interferometers. As mentioned above, the statistical error in $\mathcal{A}$ is essentially uncorrelated with that in $\mathcal{M}$, ψ, or T (*i.e.*, the correlation coefficients $r_{\mathcal{A}i}$ are for all $\lesssim 10^{-4}$). Figure 7 shows the remaining correlations coefficients $r_{\mathcal{M}\psi}$, $r_{\mathcal{M}T}$, and $r_{\psi T}$ for the initial and advanced interferometers.

D. The low frequency cut-off

In order to evaluate the covariance matrix we needed to compute the six frequency moments $f_{7/3}$, $\overline{f}_{17/3}$, $\overline{f}_4$, $\overline{f}_3$, $\overline{f}_{4/3}$, and $\overline{f}_{1/3}$. The evaluation of all of these is straightforward: however, the calculation of $\overline{f}_{17/3}$ deserves special attention: at frequencies below the pendulum frequency of the LIGO masses the seismic noise PSD is proportional to f^{-4} (*cf.* eqn. 4.5): consequently, $\overline{f}_{17/3}$ diverges as f_l approaches 0 (*cf.* eqn. 3.20).

For any particular application we never encounter the divergence: there is always a low frequency cut-off in the integral 3.20 corresponding to the finite period of the observation. Even if we had access through an interferometer to the entire life history of a binary system, our model for its evolution is relevant during only a small part of its lifetime: for example, we have assumed that the orbit is circular for all times (when in fact gravitational radiation may be responsible for circularizing it), that the evolution of the orbit is due exclusively to the gravitational forces acting between the two components, and that the two bodies are bound in a binary into the infinite past. Similarly, our model of the detector noise PSD $S_h(f)$ is not necessarily valid at very low frequencies. Nevertheless, the divergence of $\overline{f}_{17/3}$ tells us something interesting about the observation of a binary system in gravitational radiation and it is worthwhile to spend a few moments understanding its origin. So, for the purpose of understanding this divergence we assume that we know $S_h(f)$ as f tends to 0, that our

model for the waveform from a binary is correct throughout its life history, and that the lifetime of a binary extends into the infinite past.

Turn first to the related example of a strictly monochromatic signal of frequency f_0:

$$m(t) = A\cos 2\pi f_0 t \tag{5.20}$$

for all t. The noise PSD of the detector is given by $S_h(f)$. If we observe the signal for a finite period of time τ, the SNR ρ^2 is

$$\rho^2 = \frac{\tau A^2}{S_h(f_0)}. \tag{5.21}$$

No matter how small A^2 is compared to the power in the noise, the signal can always be discerned given a long enough observation time. The situation with binary inspiral is similar: consider the transformation of the time coordinate [25]

$$t' \equiv -\mathcal{M}\left(\frac{T-t}{5\mathcal{M}}\right)^{5/8}. \tag{5.22}$$

In terms of t', the signal can be expressed

$$h(t) = \frac{\mathcal{A}\mathcal{M}}{4}\left(-\frac{\mathcal{M}}{t'}\right)^{5/32}\cos(\Phi+\varphi) \tag{5.23a}$$

$$\Phi(t') = 2\pi f' t' \tag{5.23b}$$

$$f' = \frac{1}{2\pi\mathcal{M}}. \tag{5.23c}$$

Thus, the signal from an inspiralling binary is very much like that from a monochromatic source of radiation, save that

1. The signal amplitude tends to zero as the stretched time t' tends to $-\infty$;
2. The detector noise amplitude tends to ∞ as the stretched time t' tends to $-\infty$; and
3. The signal ends at $t' = 0$.

As a result, as long as the ratio of the signal amplitude to the noise PSD does not decrease too rapidly with decreasing frequency (the precise rate determined by the rate at which the frequency changes with time), then ρ^2 for a inspiralling binary system should increase without bound as the observation period extends into the infinite past. This is the role that the moment $f_{7/3}$ plays in equation 2.4 for ρ^2: if the detector noise PSD increases as or less rapidly than $f^{-7/3}$ as $f \to 0$, then $f_{7/3}$ diverges as the observation period is extended into the infinite past (*i.e.*, as the cut-off frequency f_l tends to zero) and the SNR increases without bound. In the case of LIGO, the PSD owing to seismic noise increases as f^{-4} at frequencies below the suspension pendulum frequency, so that even an infinite observation period leads to a finite SNR.

Like the SNR, the frequency f_0 of a truly monochromatic signal (*i.e.*, eqn. 5.20) can be determined to arbitrary precision given a sufficiently long observation period. By analogy,

this is equivalent to the determination of the mass parameter $\mathcal{M}$ of a inspiralling binary system (*cf.* eqn. 5.23c). Consequently, we expect that as long as the ratio of the signal amplitude to the noise PSD does not increase too rapidly, the variance in the $\mathcal{M}$ decreases to zero as the observation period extends into the infinite past. Too rapidly, in this case, is $f^{-17/3}$. Thus, *even though the signal power in a given bandwidth may be much lower than the noise power in the same bandwidth, the information present can still play an important role in determining the precision with which the parameterization of the signal can be determined.*

Again, we emphasize that these conclusions refer only to the idealized case of a circular binary system of two point masses evolving exclusively owing to the emission of quadrupole gravitational radiation. The relevance of these conclusions is that the limit $f_l \to 0$ (*i.e.*, $\overline{f}_{17/3} \to \infty$), which may seem far from the reality of observation, is in fact very close to that which can be attained in LIGO *operating in a regime where all our approximations are valid.*

In the limit $f_l \to 0$ ($\overline{f}_{17/3} \to \infty$), the variance σ_ζ^2 and the correlation coefficients $r_{i\zeta}$ vanish, corresponding to the determination of $\mathcal{M}$ to infinite precision. The remaining variances are (*cf.* eqns. 3.22a, 3.22c, 3.22d)

$$ {}_\infty\sigma_\eta^2 = \rho^{-2} \tag{5.24a} $$

$$ {}_\infty\sigma_\psi^2 = \frac{\overline{f}_{1/3}}{\overline{f}_{1/3} - \overline{f}_{4/3}^2} \frac{1}{\rho^2} \tag{5.24b} $$

$$ {}_\infty\sigma_T^2 = \left[4\pi^2\rho^2 \left(\overline{f}_{1/3} - \overline{f}_{4/3}^2\right)\right]^{-1}, \tag{5.24c} $$

and the remaining correlation coefficients are (*cf.* eqns. 3.23b, 3.23c, 3.23f)

$$ {}_\infty r_{\eta\psi} = 0 \tag{5.25a} $$

$$ {}_\infty r_{\eta T} = 0 \tag{5.25b} $$

$$ {}_\infty r_{\psi T} = \frac{\overline{f}_{4/3}}{\overline{f}_{1/3}^{1/2}}. \tag{5.25c} $$

In this limit, the moments $f_{7/3}$, $\overline{f}_{4/3}$, and $\overline{f}_{1/3}$ describe completely the precision with which $\mathcal{A}$, ψ, and T can be measured. For LIGO/VIRGO-like interferometers, these moments change negligibly when we pass from $f_l = 10$ Hz to the limit of $f_l = 0$ Hz [recall that we are assuming $S_h(f) \propto f^{-4}$ at frequencies below the resonant frequencies of the seismic isolation circuit]; consequently, in observing more than the last several minutes of binary inspiral the SNR of the observed signal is unchanged, and the variances and correlation coefficients are independent of the details of the ultralow frequency behavior of the interferometers.

By analogy with Σ_ψ and Σ_T we define ${}_\infty\Sigma_\psi$ and ${}_\infty\Sigma_T$:

$$ {}_\infty\sigma_\psi = \left(\frac{8}{\rho}\right) {}_\infty\Sigma_\psi \begin{cases} 0.232\,\text{rads} & \text{initial interferometer,} \\ 0.190\,\text{rads} & \text{advanced interferometer,} \end{cases} \tag{5.26a} $$

$$ {}_\infty\sigma_T = \left(\frac{8}{\rho}\right) {}_\infty\Sigma_T \begin{cases} 1.32 \times 10^{-4}\,\text{s} & \text{initial interferometer} \\ 2.71 \times 10^{-4}\,\text{s} & \text{advanced interferometer,} \end{cases} \tag{5.26b} $$

$$ {}_{\infty}\Sigma_{\psi} = \left[\left(\frac{\overline{f}_{1/3}}{\left(\overline{f}_{1/3} - \overline{f}^{2}_{4/3}\right)} \right) \Big/ \left(\frac{\overline{f}_{1/3}}{\left(\overline{f}_{1/3} - \overline{f}^{2}_{4/3}\right)} \right) \Bigg|_{f_c=100\,\mathrm{Hz},\, f_l=10\,\mathrm{Hz}} \right]^{1/2} \tag{5.26c} $$

$$ {}_{\infty}\Sigma_{T} = \left\{ \frac{\left[\left(\overline{f}_{1/3} - \overline{f}^{2}_{4/3}\right)\right]\Big|_{f_c=100\,\mathrm{Hz},\, f_l=10\,\mathrm{Hz}}}{\left(\overline{f}_{1/3} - \overline{f}^{2}_{4/3}\right)} \right\}^{1/2} . \tag{5.26d} $$

The factor ${}_{\infty}\Sigma_T$ is shown together with Σ_T in figure 6 for both the initial and advanced interferometers. Over the range $50\,\mathrm{Hz} < f_c < 1\,\mathrm{Khz}$ the differences between ${}_{\infty}\Sigma_i$ and Σ_i are small.

Since the SNR is unchanged as the observation period expands from the last several minutes of binary inspiral to include the entire lifetime of the binary, observations over more than the last several minutes of the lifetime of a binary system will have an insignificant effect on the number of binaries observed (*cf.* eqn. 5.5). Comparing the expressions given above for ${}_{\infty}\sigma_i$ with those for σ_i (*cf.* eqns. 3.22a–3.22d) shows that increasing the observation period increases the precision with which T can be determined by approximately 10% and the precision with which ψ can be measured a factor of two.

VI. CONCLUSIONS

Inspiralling binary systems of compact objects are regarded as the most certain observable source of gravitational radiation for the the Laser Interferometer Gravitational-wave Observatory (LIGO). As a start toward understanding the capabilities of the LIGO instruments in observations of inspiralling binary systems, we have investigated the sensitivity of a single interferometer of the LIGO type to the gravitational radiation from inspiralling binary systems in the quadrupole approximation.

Observation of binary inspiral in a single LIGO/VIRGO-like interferometer can, in principle, determine a characteristic mass $\mathcal{M}$, signal amplitude $\mathcal{A}$, time T, and phase ψ. The mass $\mathcal{M}$ is a function only of the masses of the system's components and its cosmological redshift. The amplitude $\mathcal{A}$ is inversely proportional to its luminosity distance and depends also on a function of four angles describing the relative orientation of the binary and the interferometer. The time T is related to the moment of binary coalescence. Finally, ψ is related to the phase of the binary system at a fixed moment of time and is also a function of the relative orientation angles.

The probability that the detector response is consistent with the presence of a signal from an inspiralling binary system is related to the signal-to-noise ratio (SNR) ρ that characterizes the observation. In practice, a threshold ρ_0 is chosen and we assert that a signal is present in the detector output only if $\rho \geq \rho_0$. We characterize our uncertainty in the parameters $\tilde{\boldsymbol{\mu}} = \{\tilde{\mathcal{A}}, \tilde{\mathcal{M}}, \tilde{\psi}, \tilde{T}\}$ that describe the detected binary system by defining volumes $V(P)$ in parameter space such that $\tilde{\boldsymbol{\mu}} \in V(P)$ with probability P.

When ρ^2 is large, the probability density from which $V(P)$ is constructed is a multivariate Gaussian. Consequently, the determination of $V(P)$ is equivalent to the determination of the several variance and correlation coefficients that describe the Gaussian. These coefficients

in turn describe the statistical uncertainty in the determination of $\mathcal{A}$, $\mathcal{M}$, ψ, and T, and the correlation in the errors in each.

For observations of binary systems in LIGO/VIRGO-like interferometers, the expected SNR, variance, and correlations coefficients may be expressed in terms of the mode of the probability distribution $P(\boldsymbol{\mu})$ and several moments of the noise PSD of the interferometer We have used a detailed model of the PSD for both the initial and advanced LIGO interferometers configured for standard recycling, and have evaluated the moments of the PSD, the expected SNR, variances, and correlation coefficients as functions of the recycling knee frequency.

The two interferometers of the LIGO detector share nearly the same orientation. Consequently they will act similarly to a single, more sensitive interferometer. In addition to providing results for a single interferometer of the LIGO/VIRGO type (either initial or advanced), we also express our results for the LIGO two-interferometer network in the limit that the interferometers share exactly the same orientation.

From the expected SNR and an estimate for the cosmological rate density of inspiralling binary systems we have calculated the rate of observed binary inspiral events as a function of the SNR threshold. *We find that for the advanced LIGO detector a conservative estimate of the rate of observed binary neutron star inspiral events is 69* yr^{-1}*, of which 7 per year will be from binaries at distances greater than 950 Mpc.* This is important for observational cosmology, since the differential rate (*i.e.,* $d\dot{N}/d\mathcal{A}d\mathcal{M}$) depends on the Hubble constant and other cosmological parameters [16].

For observed binary systems, the fractional standard deviation in the characteristic waveform amplitude is equal to $1/\rho$: if the threshold ρ is 8, then the fractional one-sigma uncertainty in the measured amplitude will be less than 12.5% for sources observed in either LIGO or LIGO-like interferometers. The chirp mass can be measured to phenomenal precision: again, if the threshold ρ is 8 then the fractional one-sigma uncertainty in $\mathcal{M}$ will be less than 2.2×10^{-5} for binary neutron star systems observed in the advanced LIGO detector. We have also calculated the precision with which T and ψ can be determined.

The optimum detector configuration for the observation of binary inspiral depends sensitively on the goal of the observation. For example, if the object is to maximize the rate of observed binary systems without constraining the uncertainties in $\mathcal{A}$, $\mathcal{M}$, T and ψ, then one detector configuration is clearly favored. On the other hand, if the object is to be able to characterize as precisely as possible one of the observables (*e.g.,* $\mathcal{M}$), while allowing that some otherwise observable sources may be missed entirely, then another detector configuration is preferred. We have given a concrete formulation to the question of optimum interferometer configuration and answered it in the context of our model for the interferometer noise PSD.

The quadrupole approximation is useful for our LIGO/VIRGO appraisals; however, the neglect of post-Newtonian contributions (including spin-orbit and spin-spin interactions) to the gravitational radiation luminosity and waveform is a weakness of our estimates and should be remedied in a more detailed appraisal of interferometer sensitivity[6]. Including

[6]Preliminary Monte Carlo investigations by Cutler [50] suggest that the inclusion of some of the

these interactions will increase the information that can be extracted from gravitational radiation observations of binaries over that described here. The formalism that we have developed — where the SNR, variances, and correlation coefficients are all expressed in terms of moments of the interferometer noise PSD — should prove valuable in that regard: it is readily extended to encompass an arbitrarily more sophisticated gravitational radiation waveform that is richer in information regarding the source than the one we have studied here.

ACKNOWLEDGMENTS

We would like to thank Curt Cutler, Eanna Flanagan, Tom Loredo, Kip Thorne, Ira Wasserman, and Stan Whitcomb for helpful discussions. L. S. Finn would like to thank the Alfred P. Sloan Foundation for their generous support, and D. Chernoff would like to thank the National Science Foundation for his support as a Presidential Young Investigator. This work was supported at Northwestern University by NASA grant NAGW-2936 and at Cornell University by NSF grant AST-8657467 and NASA grant NAGW-2224.

---

terms neglected in our analysis increase the fractional one-sigma uncertainty in $\mathcal{M}$ by no more than a factor of ten over our estimate, and have a much smaller effect on $\mathcal{A}$, T, and ψ.

REFERENCES

[1] R. E. Vogt, The U.S. LIGO Project, Caltech LIGO preprint 91-7, 1991.
[2] A. Abramovici *et al.*, Science **256**, 325 (1992).
[3] C. Bradaschia *et al.*, Nucl. Instrum. Methods Phys. Research **A289**, 518 (1990).
[4] E. S. Phinney, Astrophys. J. **380**, L17 (1991).
[5] R. Narayan, T. Piran, and A. Shemi, Astrophys. J. Lett. **379**, L17 (1991).
[6] P. C. Peters and J. Mathews, Phys. Rev. B **131**, 435 (1963).
[7] L. Blanchet and G. Schafer, Mon. Not. R. Astron. Soc. **239**, 845 (1989).
[8] C. W. Lincoln and C. M. Will, Phys. Rev. D **42**, 1123 (1990).
[9] T. Damour and B. R. Iyer, Ann. Inst. H. Poincaré **54**, 115 (1991).
[10] A. G. Wiseman and C. M. Will, Phys. Rev. D **44**, R2945 (1991).
[11] A. G. Wiseman, Phys. Rev. D **46**, 1517 (1992).
[12] L. E. Kidder, C. M. Will, and A. G. Wiseman, Class. Quantum Grav. **9**, L125 (1992).
[13] K. S. Thorne, (private communication), 1992.
[14] B. F. Schutz, Nature (London) **323**, 310 (1986).
[15] A. Krolak and B. F. Schutz, Gen. Relativ. Gravit. **19**, 1163 (1987).
[16] D. F. Chernoff and L. S. Finn, (unpublished), 1992.
[17] J. P. A. Clark and D. M. Eardley, Astrophys. J. **215**, 311 (1977).
[18] J. P. A. Clark, in *Sources of Gravitational Radiation*, edited by L. L. Smarr (Cambridge University Press, Cambridge, 1979), pp. 447–459.
[19] B. J. Meers, Phys. Rev. D **38**, 2317 (1988).
[20] J.-Y. Vinet, B. Meers, C. N. Man, and A. Brillet, Phys. Rev. D **38**, 433 (1988).
[21] B. J. Meeres, Phys. Lett. A **142**, 465 (1989).
[22] S. V. Dhurandhar, A. Krolak, and J. A. Lobo, Mon. Not. R. Astron. Soc. **237**, 333 (1989).
[23] P. R. Saulson, Phys. Rev. D **42**, 2437 (1990).
[24] B. J. Meers, Phys. Rev. Lett. **66**, 1391 (1991).
[25] S. Smith, Phys. Rev. D **36**, 2901 (1987).
[26] S. V. Dhurandhar, A. Krolak, and J. A. Lobo, Mon. Not. R. Astron. Soc. **238**, 1407 (1989).
[27] J. A. Lobo, Mon. Not. R. Astron. Soc. **247**, 573 (1990).
[28] A. Krolak, J. A. Lobo, and B. J. Meers, Phys. Rev. D **43**, 2470 (1991).
[29] B. S. Sathyaprakash and S. V. Dhurandhar, Phys. Rev. D **44**, 3819 (1991).
[30] P. Jaranowski and A. Krolak, Astrophys. J. **394**, 586 (1992).
[31] C. S. Kochanek, Astrophys. J. **398**, 234 (1992).
[32] L. Bildsten and C. Cutler, Tidal interactions of inspiraling compact binaries, Caltech Goldenrod Preprint GRP-303, 1992.
[33] W. Junker and G. Schafer, Mon. Not. R. Astron. Soc. **254**, 146 (1992).
[34] L. S. Finn, Phys. Rev. D **46**, 5236 (1992).
[35] A. V. Oppenheim, A. S. Willsky, and I. T. Young, *Signals and Systems* (Prentice-Hall, Englewood Cliffs, NJ, 1983).
[36] M. H. A. Davis, in *Gravitational Wave Data Analysis*, edited by B. F. Schutz (Kluwer, Dordrecht, 1989).

[37] L. A. Wainstein and L. D. Zubakov, *Extraction of Signals from Noise* (Prentice Hall, Englewood Cliffs, New Jersey, 1962).
[38] J. C. Hancock and P. A. Wintz, *Signal Detection Theory* (McGraw-Hill, New York, 1966).
[39] G. H. Golub and C. F. Van Loan, *Matrix Computations, 2nd Edition* (Johns Hopkins University Press, Baltimore, 1989).
[40] K. S. Thorne, in *300 Years of Gravitation*, edited by S. Hawking and W. Israel (Cambridge University Press, Cambridge, 1987), pp. 330–458.
[41] C. Cutler, L. S. Finn, E. Poisson, and G. J. Sussman, Gravitational radiation from a point particle in circular orbit around a black hole. II: Numerical results for the non-rotating case, Caltech Goldenrod Preprint GRP-317 in Theoretical Astrophysics, Gravitational Physics, or Quantum Optics, 1992, to appear in Physical Review D.
[42] C. Cutler *et al.*, The last three minutes: Issues in gravitational wave measurements of coalescing compact binaries, Caltech Goldenrod Preprint GRP316 in Theoretical Astrophysics, Gravitational Physics, or Quantum Optics, 1992.
[43] D. E. Knuth, *The Art of Scientific Computing: Seminumerical Algorithms* (Addison-Wesley, Reading, Massachusetts, 1981).
[44] W. H. Press, B. P. Flannery, S. A. Teukolsky, and W. T. Vetterling, *Numerical Recipes (FORTRAN Version)* (Cambridge University Press, Cambridge, 1989).
[45] P. R. Saulson, Phys. Rev. D **30**, 732 (1984).
[46] R. E. Vogt *et al.*, Proposal to the National Science Foundation, California Institute of Technology (unpublished).
[47] C. Bradaschia *et al.*, in *Gravitation: A Banff Summer Institute*, edited by R. Mann and P. Wesson (World Scientific, Singapore, 1991).
[48] S. Whitcomb, Private communication, 1992.
[49] B. Paczyński and K. Long, Astrophys. J. **333**, 694 (1988).
[50] C. Cutler, (unpublished), 1992.

FIGURES

FIG. 1. The noise power spectral density (PSD) $S_h(f)$ for the (anticipated) initial LIGO interferometers configured for standard recycling with a knee frequency of 300 Hz. The solid line shows the total PSD, while the dashed lines show the important physical limits and environmental influences that contribute to the total. For more detail, see Sec. IV A and table II.

FIG. 2. The noise power spectral density (PSD) $S_h(f)$ for the (anticipated) advanced LIGO interferometers configured for standard recycling with a knee frequency of 100 Hz. The solid line shows the total PSD, while the dashed lines show the important physical limits and environmental influences that contribute to the total. In the limit that the two LIGO interferometers have identical orientations and we ignore the information available owing to gravitational wave burst arrival time differences, the (advanced design) LIGO detector noise PSD $S_h(f)$ is 1/2 the value shown here. For more detail, see Sec. IV A and table II.

FIG. 3. The sensitivity of a LIGO-like interferometer to the gravitational radiation from a coalescing binary system depends on the detailed characteristics of the interferometer through several moments of the inverse of the its power spectral density (PSD) $S_h(f)$. In particular, the signal-to-noise ratio (SNR) ρ^2 depends on a moment of $S_h^{-1}(f)$. Here we show how this moment (normalized to its value at a recycling frequency of 100 Hz) varies with the choice of interferometer recycling frequency. To maximize the rate at which sources are detected this quantity should be maximized. For more details see IV B.

FIG. 4. We define the range function $\mathcal{R}_\gamma$ of a LIGO-like interferometer as the distance d_L within which a fraction γ of the observable sources are expected to lie. We also define a characteristic distance $\mathcal{R}$, such that the total rate of observable sources is $4\pi\mathcal{R}^3\dot{\mathcal{N}}/3$, where $\dot{\mathcal{N}}$ is the rate density of sources (which we assume to be uniform). A conservative estimate of $\mathcal{R}$ for an advanced LIGO-like interferometer is 420 Mpc. Here we show γ as a function of $\mathcal{R}_\gamma/\mathcal{R}$. For further discussion see Sec. V B.

FIG. 5. The fractional standard deviation $\sigma_{\mathcal{M}}/\widehat{\mathcal{M}}$ of the measured mass $\mathcal{M}$ depends on the distance to the source, the relative orientation of the source and the interferometer, and a factor $\Sigma_{\mathcal{M}}(f_c)$ that depends on the interferometer configuration (*i.e.*, the recycling frequency f_c; *cf.* eqn. 5.15 and Sec. V C). Here we show $\Sigma_{\mathcal{M}}$ as a function of f_c for initial and advanced LIGO-like interferometers. In order to maximize the precision with which $\mathcal{M}$ can be determined, the recycling frequency should be chosen to minimize $\Sigma_{\mathcal{M}}$. The corresponding recycling frequency differs from that which should be chosen to maximize the *rate* of sources detected (*cf.* fig. 3). For more details, see Sec. V C.

FIG. 6. The characteristic time T (related to the moment when coalescence occurs) can be determined from pre-coalescence observations. The precision with which it can be determined depends on (among other things) a factor Σ_T (defined in Sec. V C) that encapsulates all dependence of the precision on the duration of the observation and the characteristics of the detector noise. The duration of the observation will typically be several minutes, during which time the radiation frequency will sweep from 10 Hz to approximately 1 Khz, and Σ_T assumes that the observation period is limited in this way. Here we show Σ_T as a function of the detector recycling frequency for both initial and advanced LIGO-like interferometers. An interferometer optimized to measure T as precisely as possible should minimize Σ_T. Also shown are factors ${}_\infty\Sigma_T$ for initial and advanced interferometers. These are defined identically to Σ_T except that they assume an observation period that extends over the entire life of an idealized binary system evolving only owing to the emission of gravitational radiation. The small differences between ${}_\infty\Sigma_T$ and Σ_T show that the characteristics of the interferometer do not change significantly as the observation period is lengthened beyond the last several minutes of binary inspiral. For more details, see Sec. V D.

FIG. 7. The correlation coefficients describe correlations among the statistical errors in the measurements of the parameters describing an inspiralling binary system. There is no correlation between errors in the measurement of the waveform characteristic amplitude $\mathcal{A}$ and any of the other measurable parameters. The remaining correlation coefficients are shown here, for both initial and advanced LIGO-like interferometers, as a function of the interferometer recycling frequency. For more details, see Sec. V C.

TABLES

TABLE I. The amplitude of the gravitational radiation waveform observed in a single detector depends on the relative orientation between the source and the detector through the function Θ^2 (*cf.* eqn. 3.31). The orientation angles are unknown and cannot be acertained by observation; however, their *a priori* distribution is known and consequently the *a priori* distribution of the signal amplitude for binaries at a fixed distance from the detector is also known. In this table we give the cumulative probability distribution of Θ^2, and also a function of $P(\Theta^2 > x^2)$ that arises when we evaluate the number of sources within a given distance whose signal amplitudes exceed a given threshold. For more details, see Sec. III E, V A, and V B.

$P(\Theta^2 > x^2)$	x^2	$\frac{\int_0^x dz\, z^2 P(\Theta^2 > z^2)}{\int_0^\infty dz\, z^2 P(\Theta^2 > z^2)}$
90.0%	0.240	2.00%
80.0%	0.542	6.32%
75.0%	0.707	9.06%
70.0%	0.878	12.06%
60.0%	1.250	18.82%
50.0%	1.709	27.11%
40.0%	2.283	36.98%
30.0%	3.020	48.29%
25.0%	3.485	54.54%
20.0%	4.063	61.37%
10.0%	6.144	79.48%
9.0%	6.471	81.59%
8.0%	6.832	83.75%
7.0%	7.239	85.94%
6.0%	7.701	88.18%
5.0%	8.233	90.42%
4.0%	8.857	92.64%
3.0%	9.614	94.82%
2.0%	10.589	96.91%
1.0%	11.985	98.77%
0.5%	13.054	99.52%
0.4%	13.350	99.65%
0.3%	13.682	99.77%
0.2%	14.091	99.87%
0.1%	14.284	99.95%

TABLE II. The sensitivity of LIGO depends in large measure on the details of the instrumentation, and this is expected to evolve over the lifetime of the physical plant. We consider the two extremes of detector technology that have been cited by the LIGO team in their reports [1,2]: the instrumentation that is expected to be available when the facilities first come online (initial interferometers), and that expected to be available much later (advanced interferometers).

	Initial interferometers	Advanced interferometers
Temperature (T)	300°K	300°K
Pendulum frequency (f_0)	1 Hz	1 Hz
Suspension Quality (Q_0)	10^7	10^9
End mass (m)	10 Kg	1000 Kg
End mass fundamental mode ($f_{\rm int}$)	23 KHz	5 KHz
End mass quality ($Q_{\rm int}$)	10^5	10^5
Effective laser power ($I_0\eta$)	5 W	60 W
Laser wavelength (λ)	5139Å	5139Å
Mirror losses (A^2)	5×10^{-5}	2×10^{-5}

TABLE III. The signal-to-noise ratio, the variances, and the correlation coefficients all depend on the characteristics of the interferometer through the moments of its inverse noise power spectral density (*cf.* Sec. IV A). Here we give those moments for the initial and advanced LIGO instrumentation for the two cases case where the standard recycling "knee" frequency f_c is 100 Hz and 500 Hz. In both cases, the low-frequency cut-off (determined by the duration of the observation) is 10 Hz.

		Initial Interferometers		Advanced Interferometers	
f_c	[Hz]	100	500	100	500
$\bar{f}_{7/3}$	[$\mathrm{Hz}^{-1/3}$]	5.331×10^{42}	6.520×10^{42}	1.747×10^{45}	1.353×10^{45}
$\bar{f}_{17/3}$	[$\mathrm{Hz}^{-10/3}$]	9.540×10^{-8}	7.704×10^{-8}	6.758×10^{-6}	8.267×10^{-6}
$\bar{f}_4$	[$\mathrm{Hz}^{-5/3}$]	2.059×10^{-4}	1.721×10^{-4}	1.562×10^{-3}	1.720×10^{-3}
$\bar{f}_3$	[$\mathrm{Hz}^{-2/3}$]	3.056×10^{-2}	2.775×10^{-2}	6.615×10^{-2}	6.741×10^{-2}
$\bar{f}_{4/3}$	[Hz]	2.346×10^{2}	2.939×10^{2}	8.423×10	9.536×10
$\bar{f}_{1/3}$	[Hz^2]	7.765×10^{4}	1.394×10^{5}	1.248×10^{4}	2.282×10^{4}

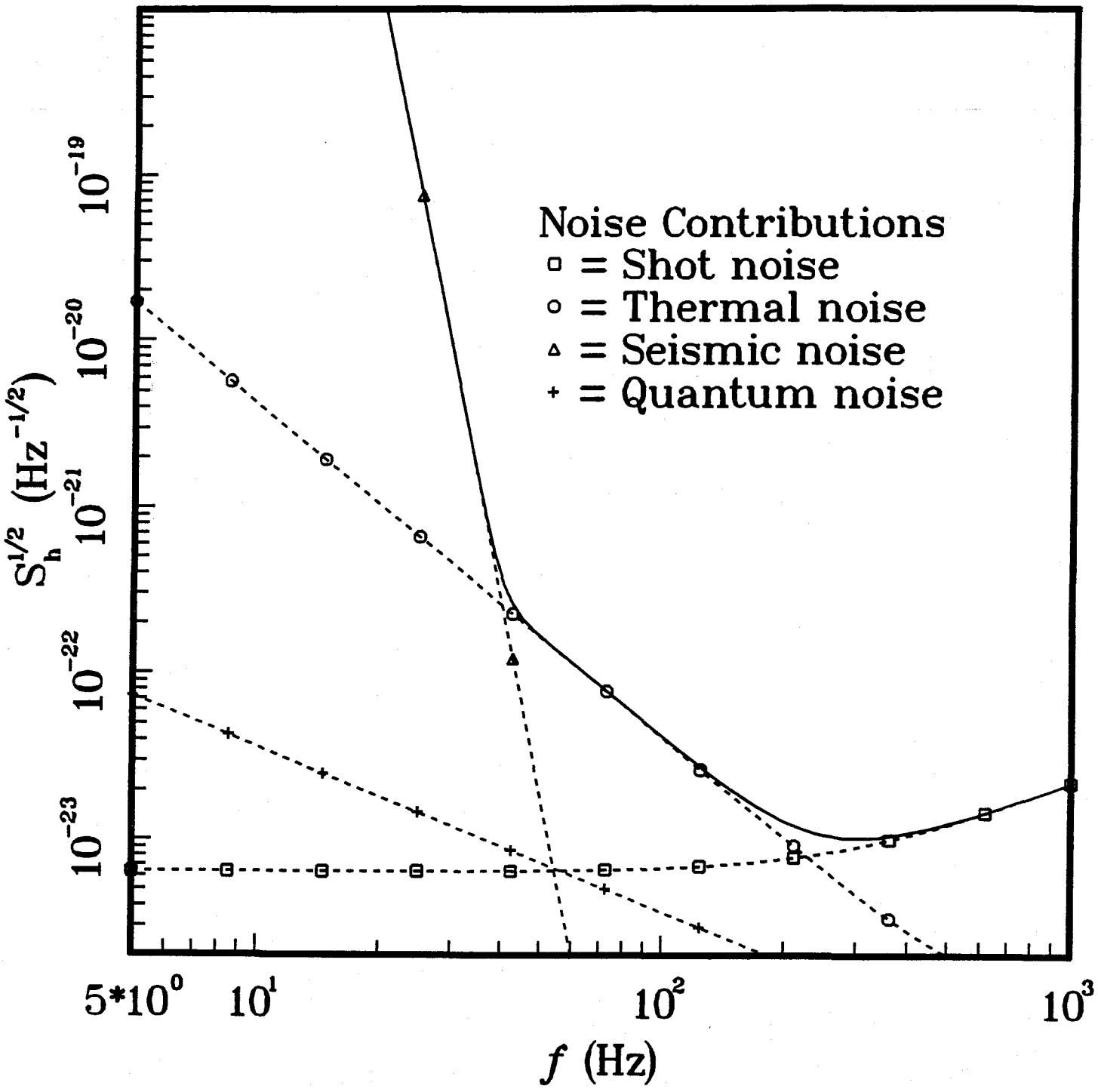
Noise Contributions
□ = Shot noise
○ = Thermal noise
△ = Seismic noise
+ = Quantum noise
$S_h^{1/2}$ (Hz$^{-1/2}$)
10^{-19}
10^{-20}
10^{-21}
10^{-22}
10^{-23}
$5*10^0$
10^1
10^2
10^3
f (Hz)

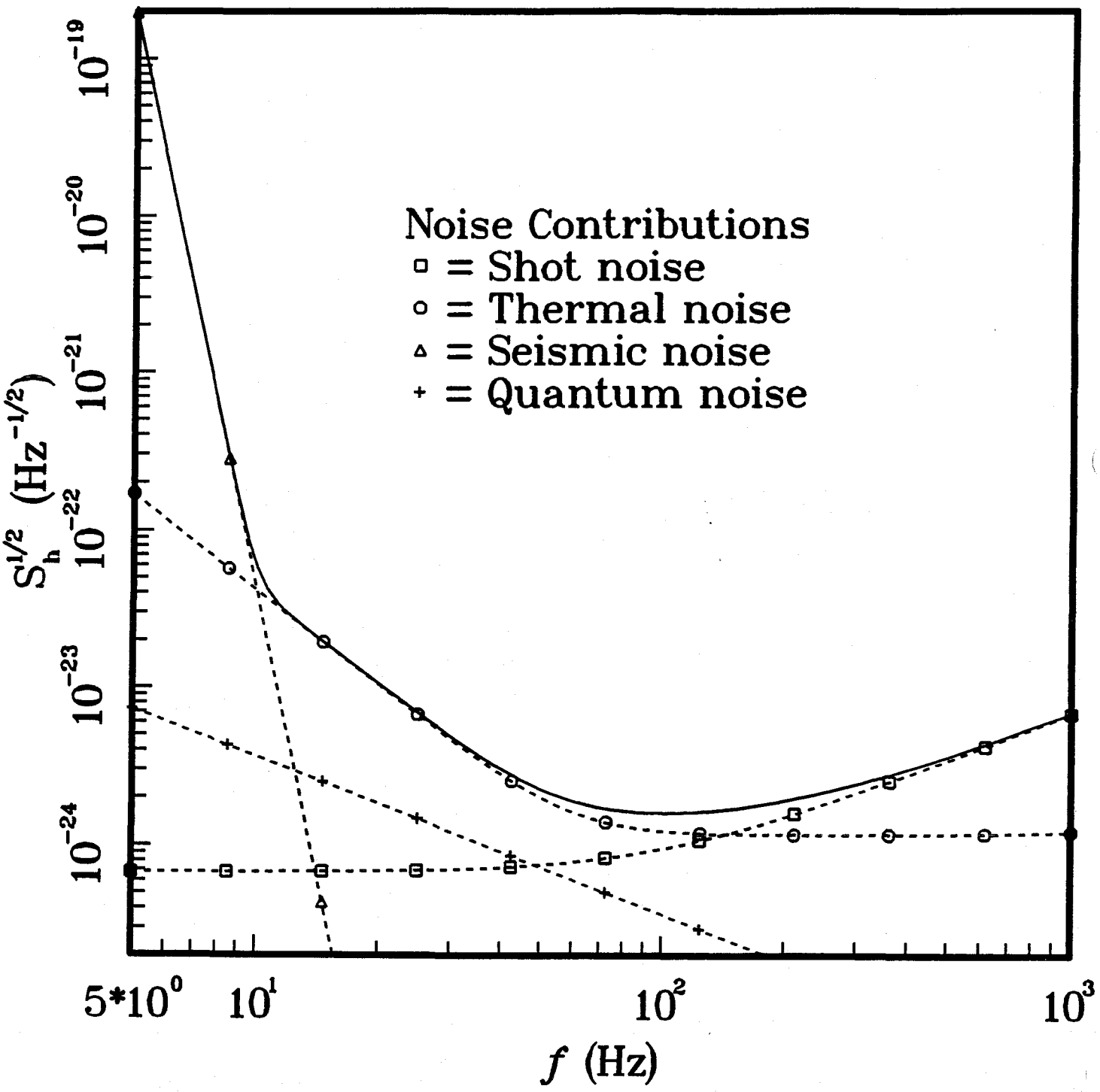
Noise Contributions
□ = Shot noise
○ = Thermal noise
△ = Seismic noise
+ = Quantum noise
$S_h^{1/2}$ (Hz$^{-1/2}$)
10^{-19}
10^{-20}
10^{-21}
10^{-22}
10^{-23}
10^{-24}
$5*10^0$
10^1
10^2
10^3
f (Hz)

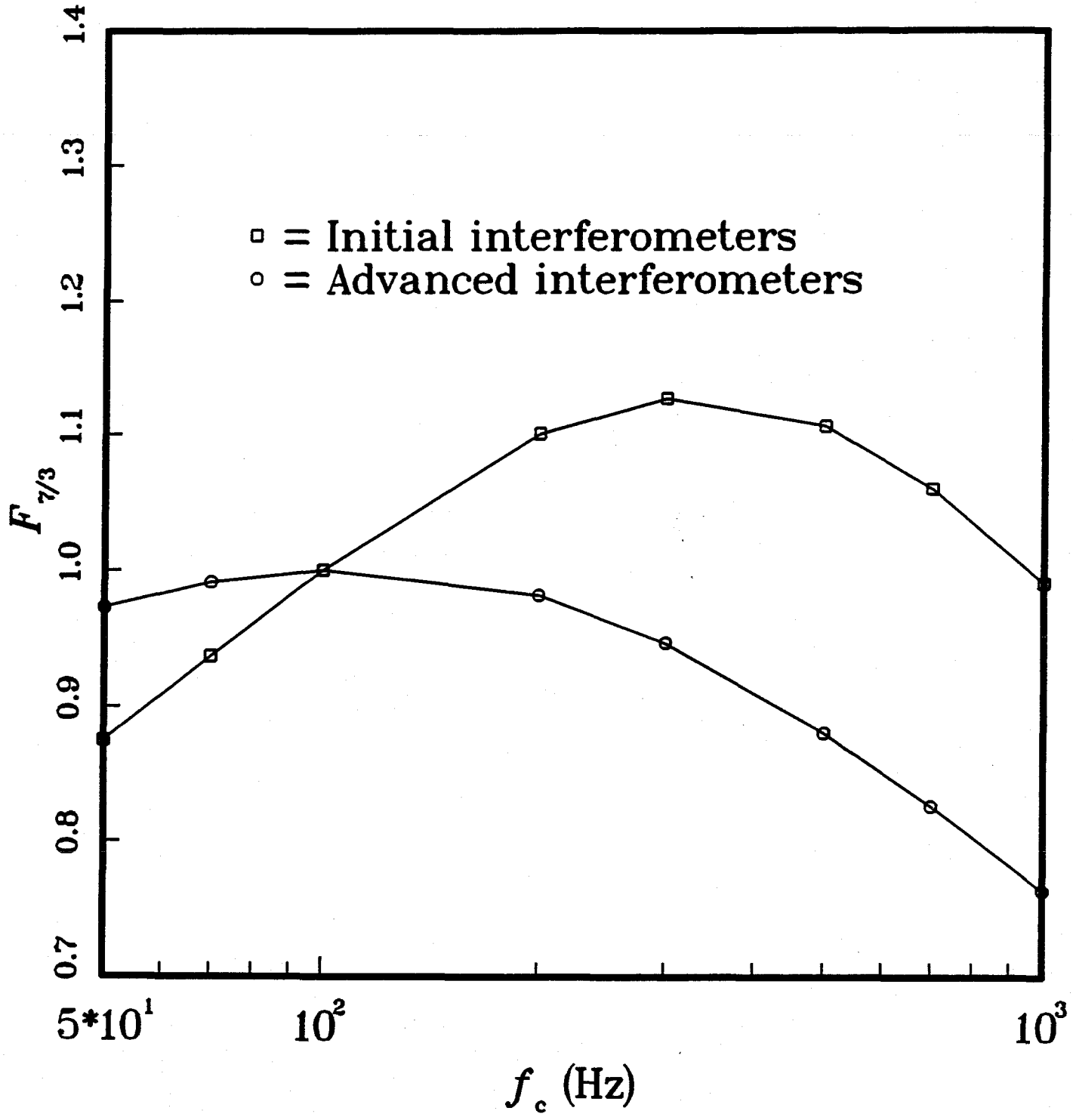
1.4
1.3
1.2
1.1
1.0
0.9
0.8
0.7
$F_{\gamma/3}$
□ = Initial interferometers
○ = Advanced interferometers
5*10^1
10^2
10^3
f_c (Hz)

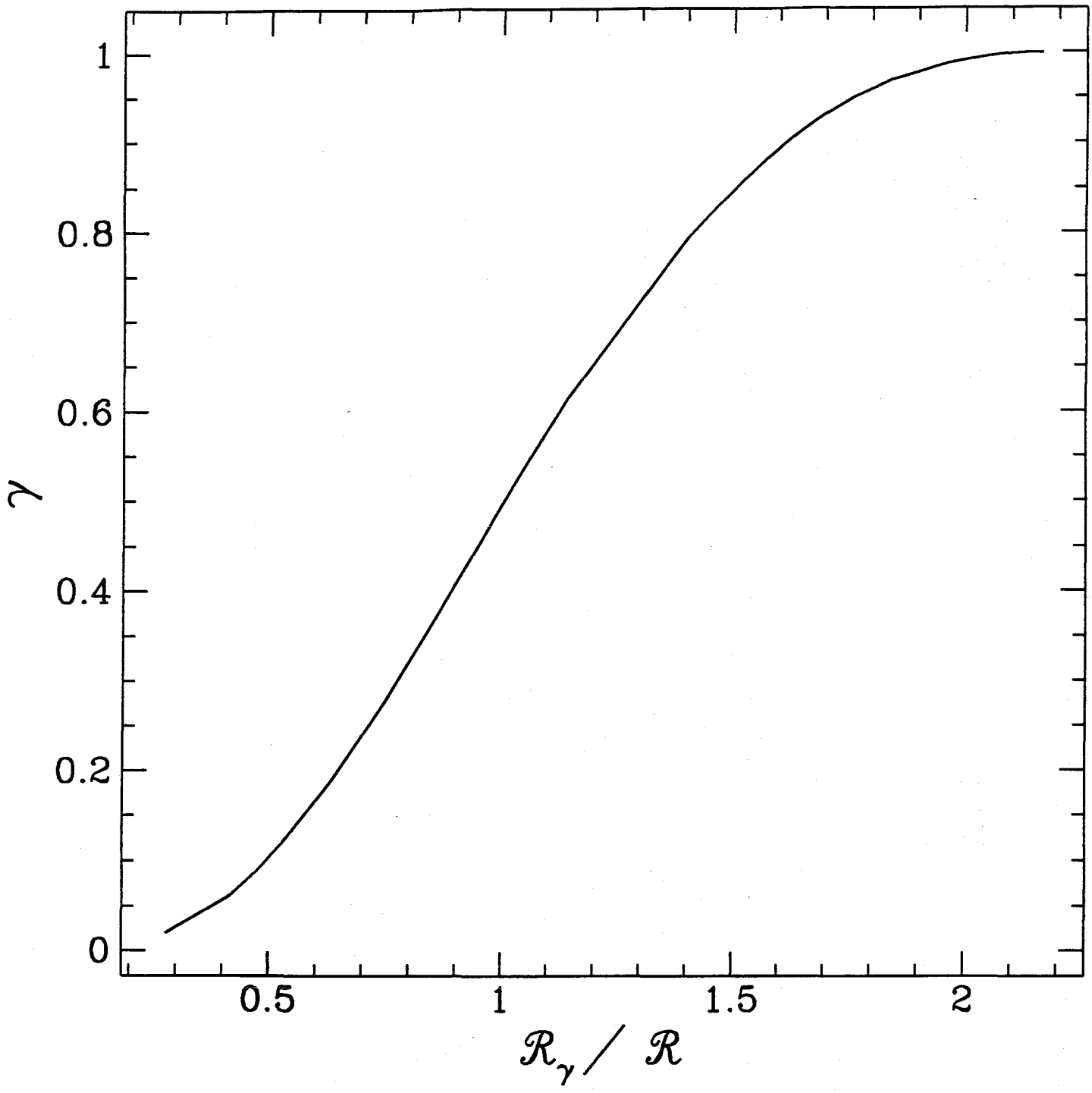
1
0.8
0.6
0.4
0.2
0
γ
0.5
1
1.5
2
$\mathcal{R}_\gamma / \mathcal{R}$

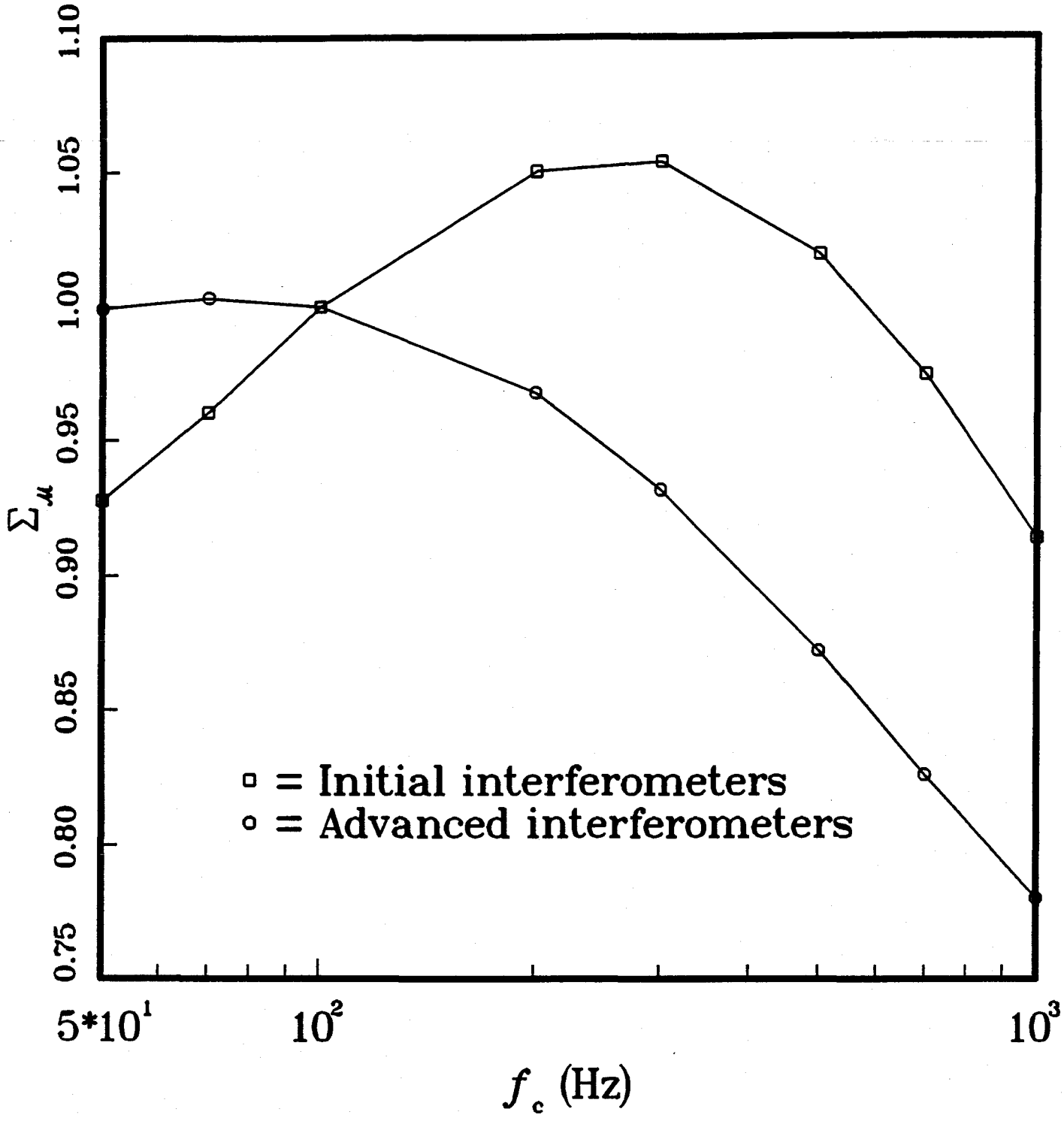
1.10
1.05
1.00
0.95
0.90
0.85
0.80
0.75
Σ_μ
□ = Initial interferometers
○ = Advanced interferometers
5*10^1
10^2
10^3
f_c (Hz)

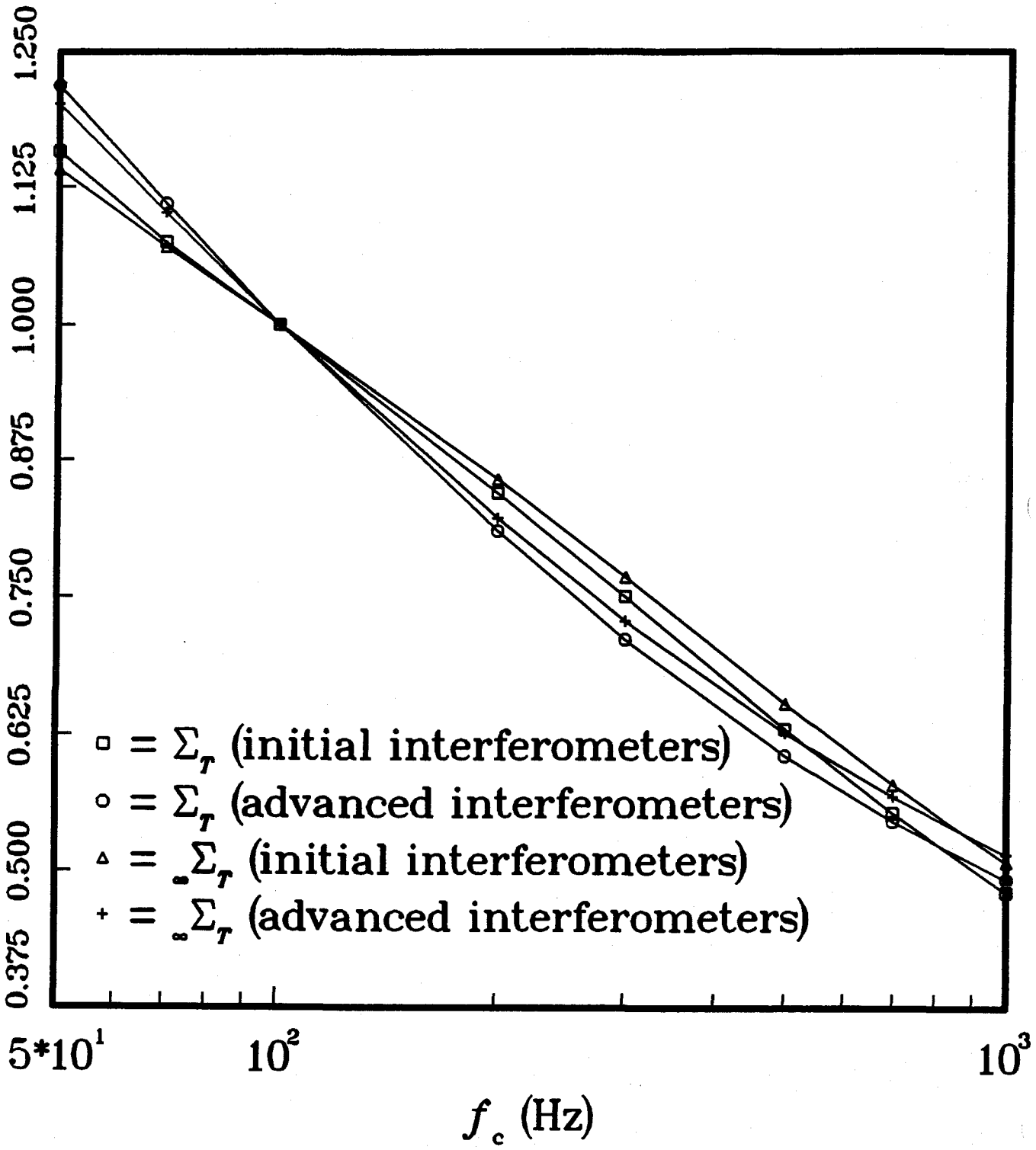
1.250
1.125
1.000
0.875
0.750
0.625
0.500
0.375
□ = Σ_T (initial interferometers)
○ = Σ_T (advanced interferometers)
△ = -Σ_T (initial interferometers)
+ = -Σ_T (advanced interferometers)
5*10^1
10^2
10^3
f_c (Hz)

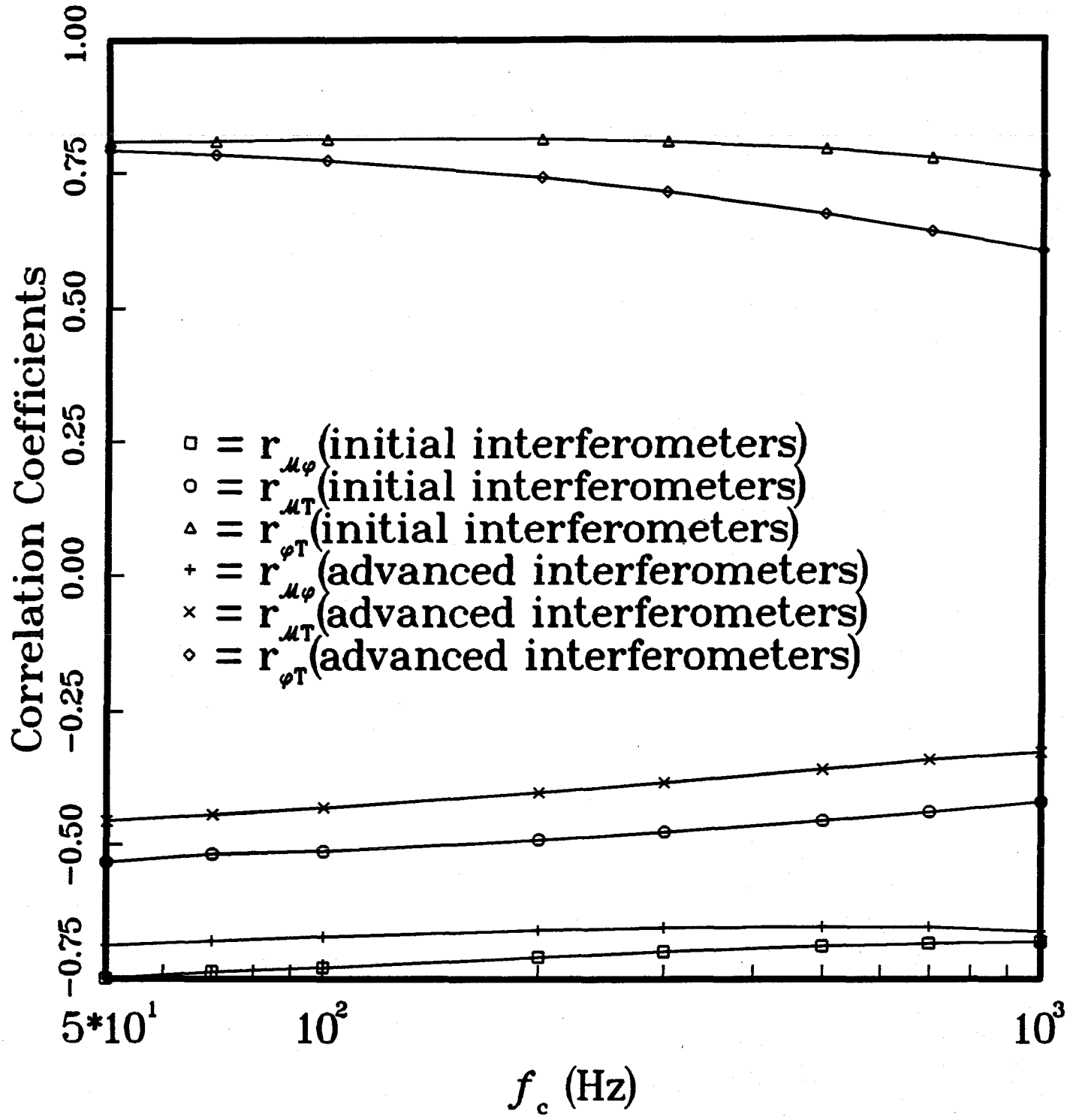
Correlation Coefficients
1.00
0.75
0.50
0.25
0.00
−0.25
−0.50
−0.75
□ = r_Mφ (initial interferometers)
○ = r_MT (initial interferometers)
△ = r_φT (initial interferometers)
+ = r_Mφ (advanced interferometers)
× = r_MT (advanced interferometers)
◇ = r_φT (advanced interferometers)
5*10^1
10^2
10^3
f_c (Hz)